Correlations between synapses in pairs of neurons slow down dynamics in randomly connected neural networks

Daniel Martí,[1] Nicolas Brunel,[2,3] and Srdjan Ostojic[1]

[1]*Laboratoire de Neurosciences Cognitives, Inserm UMR No. 960, Ecole Normale Supérieure, PSL Research University, 75230 Paris, France*
[2]*Department of Statistics and Department of Neurobiology, University of Chicago, Chicago, Illinois 60637, USA*
[3]*Department of Neurobiology and Department of Physics, Duke University, Durham, North Carolina 27710, USA*

Networks of randomly connected neurons are among the most popular models in theoretical neuroscience. The connectivity between neurons in the cortex is however not fully random, the simplest and most prominent deviation from randomness found in experimental data being the overrepresentation of bidirectional connections among pyramidal cells. Using numerical and analytical methods, we investigate the effects of partially symmetric connectivity on the dynamics in networks of rate units. We consider the two dynamical regimes exhibited by random neural networks: the weak-coupling regime, where the firing activity decays to a single fixed point unless the network is stimulated, and the strong-coupling or chaotic regime, characterized by internally generated fluctuating firing rates. In the weak-coupling regime, we compute analytically, for an arbitrary degree of symmetry, the autocorrelation of network activity in the presence of external noise. In the chaotic regime, we perform simulations to determine the timescale of the intrinsic fluctuations. In both cases, symmetry increases the characteristic asymptotic decay time of the autocorrelation function and therefore slows down the dynamics in the network.

I. INTRODUCTION

The dynamics and function of a network of neurons is to a large extent determined by its pattern of synaptic connections. In the mammalian brain, cortical networks exhibit a complex connectivity that to a first approximation can be regarded as random. This connectivity structure has motivated the study of networks of neurons connected through a random synaptic weight matrix with independent and identically distributed entries, which have become a central paradigm in theoretical neuroscience [1–3]. Randomly connected networks of firing-rate units exhibit a chaotic phase [1], which can be exploited as a substrate for complex computations [4–6]. Networks of randomly connected spiking neurons also exhibit rich dynamics that can account for the highly irregular spontaneous activity observed in the cortex *in vivo* [2,3,7,8]. Importantly, these models are to a large extent amenable to a mathematical analysis, which allows for a thorough understanding of the mechanisms underlying their dynamics.

Detailed analyses of experimental data on cortical connectivity have however identified patterns of connectivity that strongly deviate from the independent and identically distributed assumption [9–13]. The most prominent of such deviations is the overrepresentation of reciprocal connections [9,10,14] and the fact that synapses of bidirectionally connected pairs of neurons are on average stronger than synapses of unidirectionally connected pairs. These observations are consistent with a partially symmetric connectivity structure, intermediate between full symmetry and full asymmetry. How partial symmetry in the connectivity impacts network dynamics is not yet understood, in part because such partial symmetry renders the mathematical analyses more challenging [15]. Here

we study the impact of partial symmetry in the connectivity structure on the dynamics of a simple network model consisting of interacting rate units. Depending on the overall strength of coupling, such a network can display either a stable or a chaotic regime of activity, as in the random asymmetric case [1]. We examined how the degree of symmetry in the network influences the temporal dynamics in both regimes. For the stable regime, we exploited recent results from random matrix theory [16,17] to derive analytical expressions for the autocorrelation functions. These expressions demonstrate that increasing the symmetry in the network leads to a slowing down of the dynamics. Numerical simulations in the chaotic regime show a similar effect, with timescales increasing far more substantially with symmetry than in the fixed-point regime. Altogether, our results indicate that symmetry in the connectivity can act as an additional source of slow dynamics, an important ingredient for implementing computations in networks of neurons [18].

II. DESCRIPTION OF THE MODEL

We consider a network of N fully connected neurons, each described by an activation variable (synaptic current) x_i, $i = 1, \ldots, N$, obeying

$$\frac{dx_i}{dt} = -x_i + g \sum_{j=1}^{N} J_{ij}\phi(x_j), \qquad (1)$$

where g is a gain parameter that modulates the strength of recurrent connections and $\phi(\cdot)$ is the input-output transfer function that transforms activations x_i into firing rates. This transformation is nonlinear and we model it as $\phi(x) = \tanh(x)$
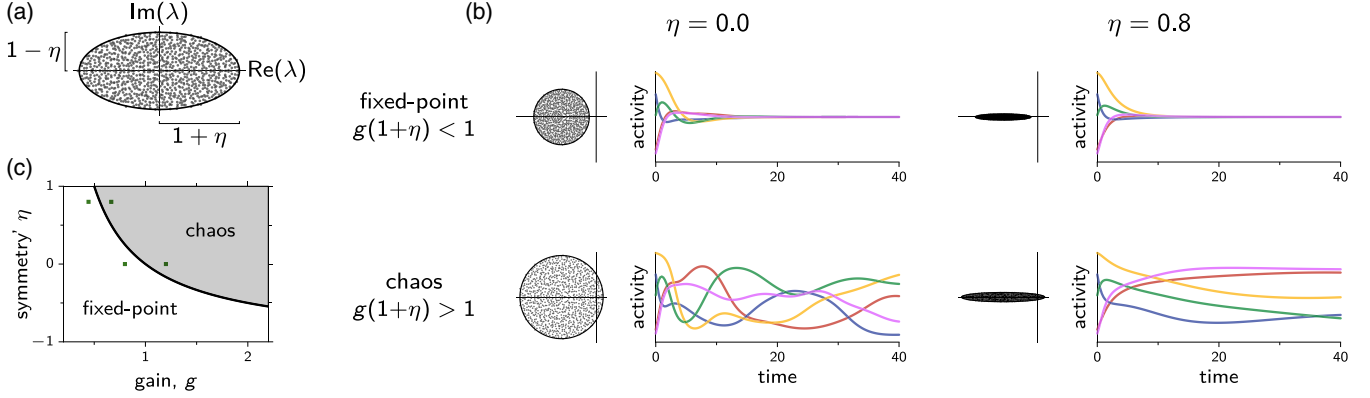
FIG. 1. (a) Spectrum of eigenvalues of a Gaussian random matrix with zero mean, variance $1/N$, and correlation coefficient η between weights connecting neuronal pairs. (b) Time evolution of the firing rates of five arbitrary neurons, for the fixed-point regime (top) and the chaotic regime (bottom), and for two different values of η (left and right panels). Next to each trajectory is the eigenspectrum of the corresponding linearized system along with the real and imaginary axes, which we include for reference. The initial firing rates were the same for all panels. All connectivity matrices were derived from a single realization of a Gaussian random matrix. To generate connectivity matrices with different η, we used the upper right and the lower left triangular portions of the Gaussian random matrix to create a symmetric and antisymmetric matrix, which we then combined to yield a **J** with the desired symmetry parameter η [for details, see the text surrounding Eq. (D4)]. (c) Activity regimes as a function of the gain and the degree of symmetry in the connections. The green squares indicate the parameter values used in (b).

for mathematical convenience (see [19–22] for studies of network models with different choices of ϕ). The elements J_{ij} of the connectivity matrix are drawn from a Gaussian distribution with zero mean, variance $1/N$, and correlation

$$[J_{ij} J_{ji}]_J = \eta/N,$$

with the square brackets $[\cdot]_J$ denoting an average over realizations of the random connections. The parameter η is the correlation coefficient between the two weights connecting pairs of neurons and quantifies the degree of symmetry of the connections. For $\eta = 0$ the elements J_{ij} and J_{ji} are independent and the connectivity matrix is fully asymmetric; for $\eta = 1$ the connectivity matrix is fully symmetric; for $\eta = -1$, it is fully antisymmetric. In Secs. II–III A we study the full range $\eta \in [-1,1]$, while in Secs. III B–IV we focus on $\eta \in [0,1]$.

III. DYNAMICAL REGIMES OF THE NETWORK

For fully asymmetric matrices, previous work has shown that the network activity described by (1) undergoes a phase transition at $g = 1$ in the limit of large N [1]. For $g < 1$ the activity for all units decays to 0, which is the unique stable fixed point of the dynamics [23], while for $g > 1$ the activity is chaotic. Such a transition can be partially understood by assessing the stability of the fixed point at $x_i = 0$ for $i = 1, \dots, N$. If we linearize Eq. (1) around this fixed point we obtain the stability matrix with components

$$M_{ij} = -\delta_{ij} + g J_{ij}. \tag{2}$$

The eigenvalues of M_{ij} are therefore those of the matrix J_{ij}, scaled by the gain g, and shifted along the real axis by -1. In the limit $N \to \infty$, for a connectivity matrix J_{ij} whose entries are independent and identically distributed Gaussian random variables of zero mean and variance $1/N$, eigenvalues are uniformly distributed in the unit disk of the complex plane [24–26]. This implies that the eigenvalues of the stability

matrix have a negative real part as long as $g < 1$ and therefore that the fixed point at 0 is stable in that range.

An analogous transition occurs when connections are partially symmetric. The presence of correlations among weights deforms the spectrum of eigenvalues into an ellipse, elongating its major radius by a factor of $1 + \eta$ and shortening the minor radius by a factor $1 - \eta$ [27–30] [Fig. 1(a)]. This property is usually referred to as the elliptic law. For the network described by (1) such a deformation causes the fixed point at $x_i = 0$ for $i = 1, \dots, N$ to lose its stability at $g = 1/(1 + \eta)$ [Figs. 1(b) and 1(c)]. In other words, symmetry lowers the critical coupling.

Our goal is to characterize how the degree of symmetry in the connections affects the network activity on each side of the instability: the relaxation response of the network at low gains and the chaotic self-generated activity observed at strong gains. Our description of the network activity will be based on the average autocorrelation function

$$C(\tau) = \frac{1}{N} \sum_{i=1}^{N} [\langle x_i(t) x_i(t + \tau) \rangle]_J, \tag{3}$$

where the average is over both the population and the realizations of the connectivity matrix [1] and where we are assuming for now that the system is stationary.

IV. DYNAMICS IN THE FIXED-POINT REGIME

A. Derivation of the autocorrelation function

In the fixed-point regime, the activity decays to zero unless the network is stimulated by external inputs. To characterize the dynamics of the network in this regime, we induce network activity by feeding each neuron with independent Gaussian white noise [31]. The amplitude of this noise is assumed to be small enough so that the synaptic activation of all neurons lies within the linear range of their input-to-rate transfer function [see Fig. 2(f) for the range of validity of that approximation].
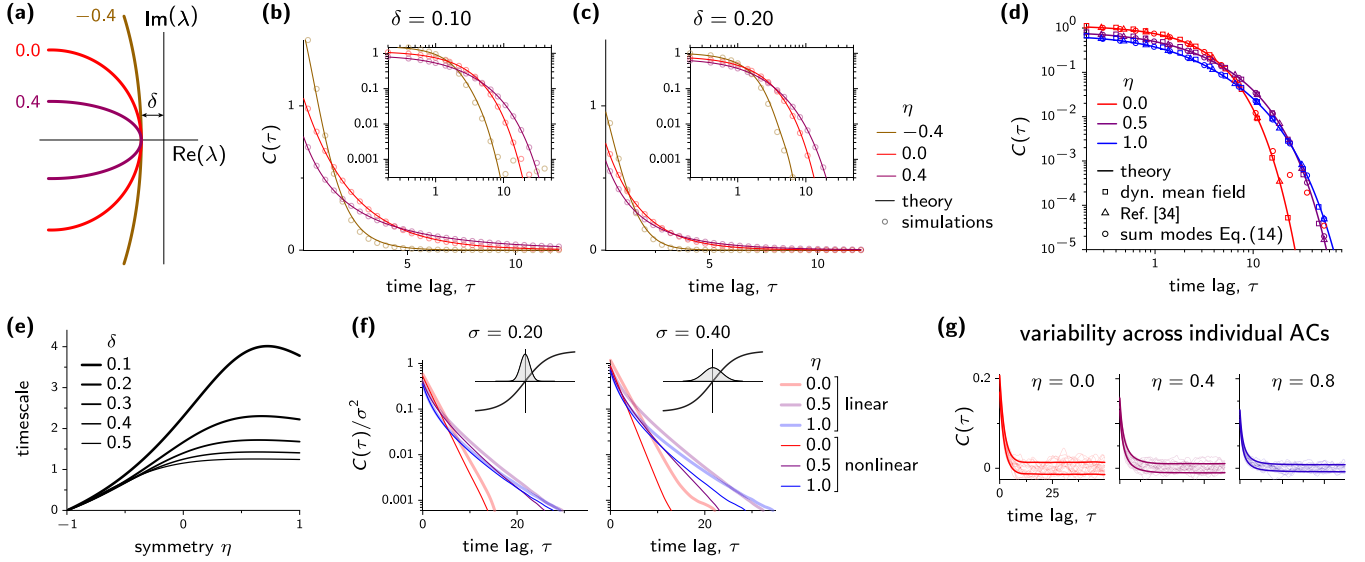
FIG. 2. (a) The distance of the eigenspectrum to the imaginary axis, or spectral gap, is kept fixed at a value δ independently of the symmetry parameter η. The color curves represent the rightmost portion of the boundaries of the eigenspectra for $\eta = -0.4, 0, 0.4$ (values indicated next to each curve). (b) and (c) Analytical prediction and numerical estimate of the average autocorrelation, for different values of the symmetry parameter η, indicated in the key. Each subplot corresponds to a particular spectral gap δ. Insets show the same curves on a log-log scale. The numerical estimate of $C(\tau)$ was derived from Eq. (3), using simulated neuronal activity generated by Eq. (4), with $N = 10\,000$ units, and averaging over time, units, and 200 different realizations of the connectivity matrix. (d) Comparison of our analytical prediction with three alternative seminumerical predictions (see the text for details). (e) Dependence on η of the timescale $\hat{\tau}$, estimated here as the mean of an unnormalized distribution defined by $C(\tau)$: $\hat{\tau} = \int_0^\infty s C(s)ds / \int_0^\infty C(s)ds$. (f) Changes in the autocorrelation function induced by the nonlinear activation function $\Phi(x) = \tanh(x)$, for two values of the amplitude of the injected noise. The inset shows noise distribution superimposed on $\Phi(x)$. Autocorrelations were numerically estimated as in (b) and (c). (g) Samples of 20 individual autocorrelation functions for three different values of η. Solid thick curves indicate the bounds of the interval [mean $-$ std, mean $+$ std], where the standard deviation was estimated from the full population of of individual autocorrelations.

Under these conditions, $\phi(x)$ can be approximated by its first-order Taylor expansion $\phi(0) + \phi'(x)|_{x=0} x = x$ and the dynamical equations become

$$\frac{d\mathbf{x}(t)}{dt} = (-\mathbf{1} + g\mathbf{J})\mathbf{x}(t) + \sigma\boldsymbol{\xi}(t), \qquad (4)$$

where $\mathbf{x}(t) = (x_1(t), \ldots, x_N(t))^T$, $\mathbf{1}$ is the identity matrix, $\mathbf{J}$ is the connectivity matrix, and $\boldsymbol{\xi}(t) = (\xi_1(t), \ldots, \xi_N(t))^T$ is a vector of independent white-noise sources of zero mean and unit variance $\langle \xi_i(t) \rangle = 0$, $\langle \xi_i(t) \xi_j(t') \rangle = \delta_{ij}\delta(t - t')$, with angular brackets representing averages over noise realizations. The parameter σ is the standard deviation of the white noise injected into neurons.

The timescales displayed by a linear system like (4) are strongly affected by the real part of the eigenvalues of the system's stability matrix and, in particular, they get longer as eigenvalues get closer to the imaginary axis. To disentangle this type of slowing down from the effects due to symmetry alone, we vary the parameter η while keeping the *spectral gap* fixed. By spectral gap we mean the distance between the spectrum of eigenvalues of the stability matrix M_{ij} [Eq. (2)] and the imaginary axis [see Fig. 2(a)]. From the elliptic law, the eigenvalue of the stability matrix with the largest real part is $z = -1 + g(1 + \eta)$ and we can keep the spectral gap at δ by setting the gain to $g = (1 - \delta)/(1 + \eta)$.

The system described by (4) is linear and can be solved by diagonalizing the connectivity matrix. The matrix $\mathbf{J}$ admits a set of right eigenvectors $\{\mathbf{R}_1, \ldots, \mathbf{R}_N\}$ that obey $\mathbf{J}\mathbf{R}_i = \lambda_i \mathbf{R}_i$

for $i = 1, \ldots, N$. These eigenvectors are in general complex valued and, except for the symmetric case $\eta = 1$, not orthogonal to one another, which implies that $\mathbf{J}$ cannot be diagonalized through a unitary transformation. Matrices of this kind are called non-normal and do not commute with their transpose conjugate: $\mathbf{J}\mathbf{J}^\dagger \neq \mathbf{J}^\dagger\mathbf{J}$ [32]. Even if non-normal matrices cannot be diagonalized by an orthogonal set of eigenvectors, it is always possible to form a biorthogonal basis by extending the set of right eigenvectors with the set of left eigenvectors, which obey $\mathbf{L}_i^\dagger \mathbf{J} = \lambda_i \mathbf{L}_i^\dagger$. This extended basis is biorthogonal in the sense that $\mathbf{L}_i^\dagger \mathbf{R}_j = \delta_{ij}$. We can summarize all these properties in a compact way by defining the square matrices $\mathbf{R}$ and $\mathbf{L}$ that result from adjoining in columns the set of, respectively, right and left eigenvectors and by introducing the diagonal matrix $\mathbf{\Lambda}$ that contains the eigenvalues λ_i of $\mathbf{J}$ in its diagonal entries. In this notation the biorthogonality condition is $\mathbf{L}^\dagger\mathbf{R} = \mathbf{1}$ and the eigenvalue equations for the right and left eigenvectors read $\mathbf{J}\mathbf{R} = \mathbf{R}\mathbf{\Lambda}$ and $\mathbf{L}^\dagger\mathbf{J} = \mathbf{\Lambda}\mathbf{L}^\dagger$.

We can now write the formal solution of (4),

$$\mathbf{x}(t) = \sigma \int_{-\infty}^t e^{(-\mathbf{1}+g\mathbf{J})(t-s)}\boldsymbol{\xi}(s)ds$$

$$= \sigma\mathbf{R} \int_{-\infty}^t e^{(-\mathbf{1}+g\mathbf{\Lambda})(t-s)}\mathbf{R}^{-1}\boldsymbol{\xi}(s)ds,$$

where in the last equality we used the basis of right eigenvectors to write $\mathbf{J} = \mathbf{R}\mathbf{\Lambda}\mathbf{R}^{-1}$ and we implicitly expanded the exponential in its power series to obtain the final result.

From this expression we can derive the population-average autocorrelation for a particular realization of the connectivity:

$$
\begin{aligned}
C_J(\tau) &= \frac{1}{N} \langle \mathbf{x}^\dagger(t)\mathbf{x}(t+\tau) \rangle \\
&= \frac{1}{N} \operatorname{Tr} \langle \mathbf{x}(t+\tau)\mathbf{x}^\dagger(t) \rangle \\
&= \frac{\sigma^2}{N} \int_0^\infty e^{-2u-\tau} \operatorname{Tr}\{\mathbf{R}^\dagger \mathbf{R} e^{g\mathbf{\Lambda}(u+\tau)} \mathbf{L}^\dagger \mathbf{L} e^{g\mathbf{\Lambda}^\dagger u}\} du.
\end{aligned}
\tag{5}
$$

In the second equality we used the cyclicity of the trace and in the last line we changed the integration variable to $u = t - s$ and we used the biorthogonality condition to write $\mathbf{R}^{-1} = \mathbf{L}^\dagger$. The average over noise amounts to applying the identity $\langle \boldsymbol{\xi}(t)\boldsymbol{\xi}^\dagger(t') \rangle = \sigma^2 \mathbf{1}\delta(t - t')$. Note that the σ^2 appears as an overall factor, so we can set $\sigma = 1$ without loss of generality.

We can simplify (5) by introducing the so-called overlap matrix, with components

$$
O_{ij} = (\mathbf{L}^\dagger \mathbf{L})_{ij}(\mathbf{R}^\dagger \mathbf{R})_{ji},
\tag{6}
$$

which characterizes the correlations between left and right eigenvectors [16]. Equation (5) then becomes

$$
C_J(\tau) = \frac{1}{N} \int_0^\infty e^{-2u-\tau} \sum_{i=1}^N \sum_{j=1}^N e^{g\lambda_i(u+\tau)} O_{ij} e^{g\bar\lambda_j u} du.
\tag{7}
$$

If the connectivity matrix were normal, the overlap would be the identity matrix and the autocorrelation (7) would just be a sum of independent contributions, one per eigenvalue. These contributions are coupled for non-normal matrices.

We can make further analytical progress by studying the autocorrelation (7) in the limit $N \to \infty$, in which the differences of $C_J(\tau)$ across realizations of the connectivity matrix disappear and the autocorrelations of all units become close to the population average [Fig. 2(g)]. In that limit sums over indices are replaced with integrals over eigenvalues, while the overlap matrix is replaced with the local average of the overlap, defined as

$$
D(z_1, z_2) = \lim_{N\to\infty} \frac{4}{N} \left[\sum_{i=1}^N \sum_{j=1}^N O_{ij} \delta^2(z_1 - \lambda_i)\delta^2(z_2 - \lambda_j) \right]_J.
\tag{8}
$$

Here $z = x + iy$ are complex numbers and we defined the complex Dirac delta as $\delta^2(z) \equiv (1/2)\delta(x)\delta(y)$ so that it satisfies the normalization condition $\int \delta^2(z)d^2z \equiv \int \delta^2(z)dz\,d\bar{z} = 1$. After taking the limit $N \to \infty$, Eq. (7) becomes

$$
C(\tau) = \int_0^\infty e^{-2u-\tau} A(u,\tau)du,
\tag{9}
$$

where we defined

$$
A(u,\tau) = \frac{1}{4} \iint e^{g(z_1+\bar{z}_2)u+gz_1\tau} D(z_1,z_2)d^2z_1 d^2z_2.
\tag{10}
$$

Each of the integrals in Eq. (10) is over complex values and involves the expression of $D(z_1, z_2)$ for the ensemble of Gaussian random matrices with partial symmetry, which was derived using diagrammatic techniques in Ref. [16] and whose functional form can be found in Appendix A. We used the

result of [16] to evaluate the double complex integral $A(u,\tau)$ in Eq. (10). The details of the evaluation are given in Appendix A and the result is

$$
A(u,\tau) = A_1(u,\tau) + A_2(u,\tau),
\tag{11}
$$

with

$$
\begin{aligned}
A_1(u,\tau) &= (1 + \eta^2)I_0(g\psi(u,\tau;\eta)) \\
&\quad - 2\eta\left(1 + \frac{2(1-\eta)^2\tau^2}{\psi(u,\tau;\eta)^2}\right)I_2(g\psi(u,\tau;\eta)),
\end{aligned}
\tag{12}
$$

$$
\begin{aligned}
A_2(u,\tau) &= \frac{-1}{g^2 u(u+\tau)} \sum_{k=1}^\infty \eta^k k^2 I_k(2g\sqrt{\eta}u) \\
&\quad \times I_k(2g\sqrt{\eta}(u+\tau)),
\end{aligned}
\tag{13}
$$

where $I_k(\cdot)$ is the modified Bessel function of order k and where in Eq. (12) we defined

$$
\psi(u,\tau;\eta) = 2\sqrt{(1+\eta)^2 u(u+\tau) + \eta\tau^2}.
$$

The autocorrelation is finally computed from Eq. (9), integrating numerically over u.

Expressions (11)–(13) are valid for the full range $-1 \leqslant \eta \leqslant 1$. For negative η we replace $\sqrt{\eta}$ with $i\sqrt{|\eta|}$ and apply the identity $I_\nu(iz) = i^\nu J_\nu(z)$, which is valid for integer ν.

The analytical prediction given by Eqs. (9) and (11)–(13) matches with the autocorrelation estimated from numerical simulations [Fig. 2(b)], although for long-time lags the numerical estimate becomes noisy due to finite-size effects. To check the validity of our prediction also at long-time lags, we compared our analytical prediction with three alternative derivations [Fig. 2(c)]. One such derivation consists of computing the autocorrelation for large but finite N, by computing numerically the eigenvalues and eigenvectors of randomly generated matrices, evaluating the time integral of Eq. (7), which gives

$$
C_J(\tau) = -\frac{1}{N} \sum_{i=1}^N \sum_{j=1}^N \frac{O_{ij} e^{-(1-g\lambda_i)\tau}}{2 + g(\lambda_i + \bar\lambda_j)},
\tag{14}
$$

and then by averaging $C_J(\tau)$ over multiple realizations of the connectivity matrix. Another derivation is based on dynamical mean-field theory [15,31,33], which gives rise to a set of integro-differential equations involving $C(\tau)$ that can be solved numerically (Appendix D). Finally, we numerically computed the inverse Fourier transform of the power spectrum derived in [34] for this same system. Bravi et al. [34] used a perturbative method to derive the system of integro-differential equations (D25) and (D26), which they solved for the correlation and response functions by using a Laplace transform. All derivations yield the same result, except for the deviations we observe when applying Eq. (14) at long τ which are caused by finite-size effects.

Our results show that an increase in symmetry tends to spread autocorrelations toward longer-time lags and that this effect gets larger the closer the system gets to the onset of chaos [Fig. 2(e)]. An intuitive explanation for this slowing down is that the deformation of the eigenspectrum caused by symmetry increases the density of eigenvalues with small imaginary parts, thereby enlarging the contribution of low-frequency modes.
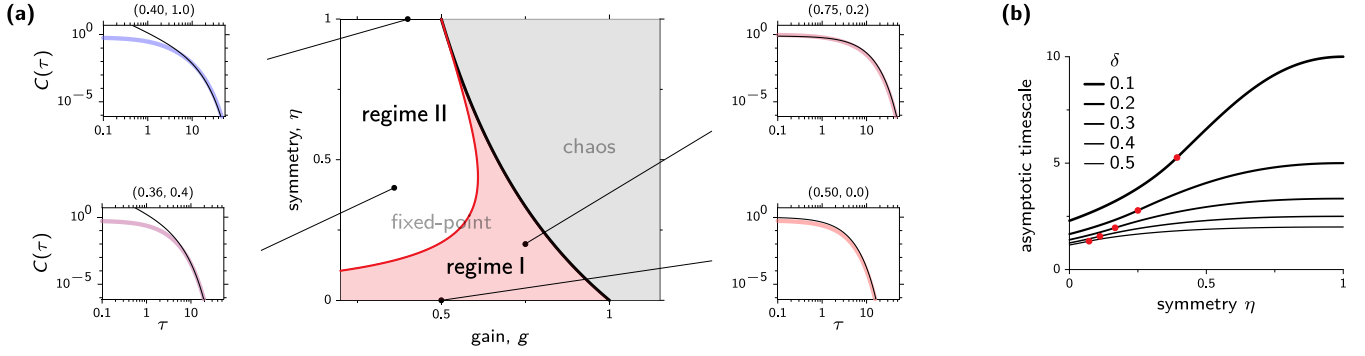
FIG. 3. (a) Phase diagram showing the different activity regimes as a function of the gain g and the degree of symmetry η (center). At both sides of the diagram, we show the autocorrelation functions at a few representative points in the (g,η) plane, indicated by the black dots in the main diagram. Each autocorrelation plot contains the exact prediction of $C(\tau)$ given by Eqs. (9)–(13) (thick colored curve) and the asymptotic approximation, summarized in Eqs. (15)–(20) (thin black curve). At the top of each such plot are the parameters g and η used. (b) Asymptotic timescale of the autocorrelation as a function of the degree of symmetry, for different spectral gaps δ. These curves were generated with the inverses of $G_{\mathrm{I,II}}(\eta,\delta)$, Eqs. (15) and (18). The red dot on each curve indicates the value of η where the transition between subregimes occurs.

B. Behavior at long-time lags

While Eqs. (9)–(13) are exact, they provide little analytical insight into how the autocorrelation depends on parameters. A more explicit dependence can be obtained by evaluating $C(\tau)$ in the limit of long τ. We relegate the details of the calculation to Appendix B and summarize the main results here. The analysis shows that, in the fixed-point regime, there exist two subregimes of activity that differ in how the asymptotic decay rate of the autocorrelation depends on the symmetry parameter η and the spectral gap δ. For small values of η and δ, the autocorrelation decays as a pure exponential at long τ (regime I),

$$C(\tau) = F_{\mathrm{I}}(\eta,\delta)e^{-\tau G_{\mathrm{I}}(\eta,\delta)}, \tag{15}$$

with

$$F_{\mathrm{I}}(\eta,\delta) = \frac{\delta^{-1/2}(1-\eta)^2}{2\sqrt{2}(1-\delta)}, \tag{16}$$

$$G_{\mathrm{I}}(\eta,\delta) = \frac{1-\eta}{1+\eta}\sqrt{2\delta - \delta^2}. \tag{17}$$

Conversely, for sufficiently large values of η and δ autocorrelation for long τ can be approximated by a power multiplied by an exponential decay (regime II)

$$C(\tau) = \tau^{-3/2}F_{\mathrm{II}}(\eta,\delta)e^{-\tau G_{\mathrm{II}}(\eta,\delta)}, \tag{18}$$

with

$$F_{\mathrm{II}}(\eta,\delta) = \frac{1}{4\sqrt{\pi}}\left(\frac{1+\eta}{1-\delta}\right)^{3/2}\left[\frac{2\eta^{-1/4}(1+\eta^2)}{\delta(1+\eta)-[1-\sqrt{\eta}]^2}\right.$$
$$\left. -\frac{\eta^{5/6}(1+\eta)}{(1-\sqrt{\eta})^2+2\sqrt{\eta}\delta}\right], \tag{19}$$

$$G_{\mathrm{II}}(\eta,\delta) = \frac{(1-\sqrt{\eta})^2 + 2\delta\sqrt{\eta}}{1+\eta}. \tag{20}$$

A comparison between the asymptotic expression in Eq. (18) and the full expression for the autocorrelation function reveals, however, that the power law is not observed in practice because the range below the cutoff falls below the values of τ

where the asymptotic approximation starts matching the exact expression.

Figure 3(a) shows the exact parameter region of each asymptotic regime, after transforming the spectral gaps into gains. In both regimes the autocorrelation's asymptotic decay rate matches the exact result for time lags longer than a few time units [see Fig. 3(a), lateral panels]. It seems therefore reasonable to associate the timescale of the autocorrelation with the inverse of $G_{\mathrm{I,II}}(\eta,\delta)$ [see Eqs. (15) and (18)], where the subindex I,II is chosen according to the subregime found at the parameter values (η,δ). The asymptotic timescale of the autocorrelation increases monotonically with symmetry regardless of the subregime the network operates in [Fig. 3(b)], although this dependence is convex in the exponential subregime and concave in the power-law-with-cutoff regime [in Fig. 3(b) see the curves split by the red dots, which mark the boundary between subregimes]. Note also that as the spectral gap δ shrinks to 0 the system enters the exponential regime and timescales diverge as $\delta^{-1/2}$, according to Eq. (17).

C. Effect of overlaps

As shown in Eq. (7), the autocorrelation function in general depends on two factors, the full eigenspectrum of the connectivity matrix and the overlaps between eigenvectors, both of which are modified when η is changed. To disentangle the effects of the changes in the eigenspectrum and the changes in eigenvector overlaps, here we compare the autocorrelation we derived in Sec. IV A with the autocorrelation we would obtain if we assumed that the eigenvectors of $\mathbf{J}$ were orthogonal. If that were the case, the autocorrelation would be computed as a sum of decoupled contributions associated with the different eigenvalues and, in particular, the distribution of eigenvectors would play no role in the result (see Sec. IV C for details). Figure 4(a) shows the predicted autocorrelations both including and excluding the contribution from the overlap (6). As expected, both predictions coincide for $\eta = 1$ and they increasingly depart from each other for decreasing values of η. To better characterize this difference we show the variance $C(0)$ as a function of the symmetry parameter for several values of the spectral gap [Fig. 4(b)]. Remarkably, the variance
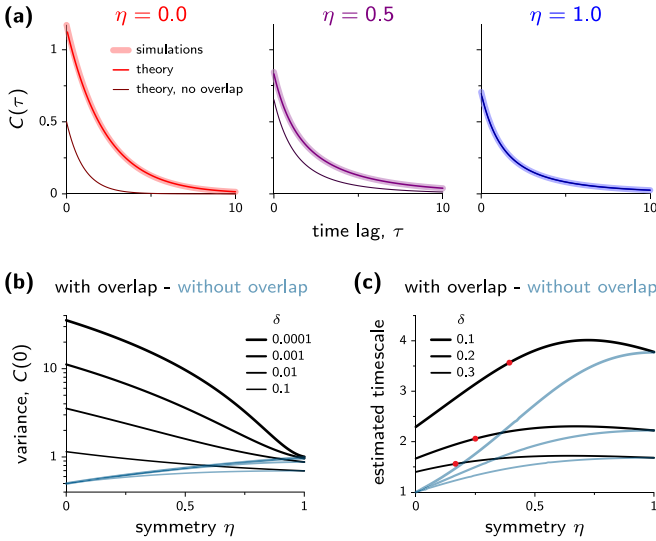
FIG. 4. Effect of overlaps on autocorrelations and timescales. (a) Analytical predictions and numerical estimations of the average autocorrelation of network activity for $\delta = 0.1$. We include two analytical predictions: the correct one, which takes properly into account the correlations among eigenvectors ["theory," based on Eq. (7) and its large-N disorder-average limit (9)], and an incorrect prediction that assumes orthogonality among eigenvectors ("theory, no overlap"). (b) Theoretical prediction of the variance of network activity, given by $C(0)$, as a function of the symmetry parameter. As in (a), we also include the prediction we would obtain if eigenvectors were orthogonal ("without overlap"). (c) Estimate of the overall timescale $\hat{\tau}$ (see the text for details), with and without taking into account the effect of overlaps. Red dots indicate the transition between asymptotic regimes, as in Fig. 3(b).

decreases with symmetry, but the opposite occurs when we remove the contribution from eigenvector overlaps [see the "with" and "without" overlap curves in Fig. 4(b)]. In both cases the variance increases as spectral gaps get smaller, which is consistent with the fact that the restoring drive towards the fixed point gets weaker as the spectral gap gets smaller. This effect is however much subtler when overlaps are not taken into account [35].

The overlap also contributes to the overall timescale of the autocorrelation, which we define by the quantity $\hat{\tau} = \int_0^\infty t C(t) dt / \int_0^\infty C(t) dt$. This definition guarantees that for an exponential autocorrelation $C(\tau) \propto \exp(-|\tau|/\tau_0)$ the overall timescale is exactly τ_0 and provides a rough estimate of a natural timescale for autocorrelations with more complex dependences. The numerical evaluation of T shows that the overall timescale is systematically smaller if the contribution of the eigenvalues is removed [Fig. 4(c)]. Unsurprisingly, either with or without the overlap contribution the timescale gets longer as the spectral gap gets smaller. Note also that the overall timescale T varies nonmonotonically with the symmetry parameter [Fig. 4(c)], unlike the asymptotic dependence shown in Fig. 3(b).

V. DYNAMICS IN THE CHAOTIC REGIME

In the chaotic regime, the network generates its own fluctuating activity without the need for external noise. Recall

that chaotic activity emerges as soon as the largest of the real parts of the eigenspectrum, given by $-\delta$ and usually called a spectral abscissa, becomes positive. We follow the strategy of the preceding section and we keep the spectral abscissa fixed while we vary the symmetry parameter η.

The evolution of firing activities shown in Fig. 5(a) suggests that in the chaotic regime the self-generated fluctuations get slower as η increases. This slowing is accompanied by an increasing tendency of firing rates to linger around the extreme values of their dynamical range, as reflected by an increasingly bimodal distribution of currents x and rates $\phi(x)$ when η increases [Fig. 5(b)]. We quantified the slowing down of the fluctuations with the population-average autocorrelation. For $\eta = 0$ the autocorrelation can be derived self-consistently in the limit of infinitely large networks, using the dynamical mean-field approach [1,19] (see also Appendix D for a general derivation). Unfortunately, this method does not lead to a closed-form solution for the autocorrelation as soon as $\eta > 0$ (see Appendix D) and we have to resort to numerical estimates, summarized in Fig. 5(c) for several values of η. For completeness we also include the autocorrelation functions for fixed gain, rather than fixed spectral abscissa [Fig. 5(d)].

The numerical estimates show that the timescale associated with the autocorrelation increases strongly as a function of η and is considerably longer than in the fixed-point regime [Fig. 5(e)]. Such a slowing is rather insensitive to whether we fix the spectral abscissa or the gain, despite the fact that the variance $C(0)$ varies far more strongly when gain is fixed [Fig. 5(d)].

Quite strikingly, for $\eta = 1$ fluctuations become slower as time goes by and our initial assumption that the activity is stationary does not hold. The population-averaged autocorrelation $C(t, t + \tau) = [x(t)x(t + \tau)]_{J,N}$ at different points in time shows that the characteristic timescale of the autocorrelation grows with t [Fig. 5(d)], a signature of aging dynamics [36]. For lower values of η, the dependence on the autocorrelation on the two timescales is less clear. Due to strong finite-size effects, it is difficult to determine from simulations alone whether aging appears also when the connectivity is not fully symmetric.

VI. DISCUSSION

In this work we examined the effect of partially symmetric connectivity on the dynamics of randomly connected networks composed of rate units. We have derived an analytical expression for the autocorrelation function in the regime of linear fluctuations around the fixed point and shown that increasing the symmetry of the connectivity leads to a systematic slowing down of the dynamics. Numerical simulations confirm that a similar phenomenon takes place in the chaotic regime of the network.

The impact of the degree of symmetry of the connectivity matrix on the dynamics of neural networks has been a long-standing question in theoretical neuroscience. Theorists initially focused on fully symmetric networks of binary spin-like neurons [37] for which tools from equilibrium statistical mechanics could be readily applied [38]. After these initial studies, the realization that brain networks are not symmetric led physicists to investigate the dynamics of networks whose connectivity matrix has a random antisymmetric component.
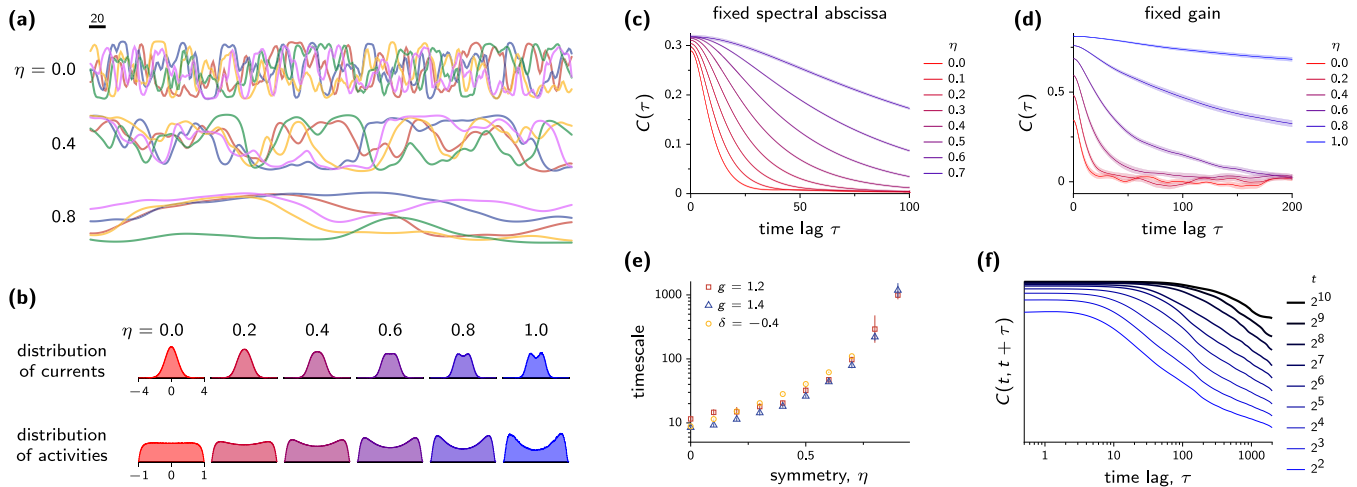
FIG. 5. Effects of symmetry in the chaotic regime. (a) Firing rates of five arbitrary units in a network of size $N = 10^4$, for three different values of η (value indicated next to each inset). The spectral gap is $\delta = -0.4$ (i.e., the spectral abscissa is 0.4). (b) Histograms of the currents x and firing activities $\phi(x)$, for different values of η. Samples were taken every 40 time units from the simulated activity of a network of 10^4 units for ten different realizations of the connectivity matrix and $\delta = -0.4$. (c) Population-average autocorrelation, for different values of the symmetry parameter η and $\delta = -0.4$. The autocorrelation was estimated from the simulated activity of a network of 10^4 units, using 200 different draws of the connectivity matrix. The estimated standard error of the mean is shown in semitransparent shade. (d) Same as in (c), but keeping the gain fixed at $g = 1.5$ instead of fixing δ. For this panel we estimated the autocorrelation using ten independent realizations of the connectivity matrix. Notice the different axis ranges with respect to (c). (e) Timescale of the network fluctuations, estimated from the width of the autocorrelation function at half of its maximum value, using the simulation results from (c) and (d). The error bars indicate the standard error of the mean. (f) Nonstationarity of the network activity for $\eta = 1$. The autocorrelation function depends on two timescales, the time lag τ and the time t, since the simulation started with an arbitrary initial condition. The autocorrelation is estimated from simulated neuronal activity of size $N = 10^4$ for $T = 3030$ time units, using five different trials with different realizations of the connectivity matrix. In this figure the gain was fixed at $g = 1.4$.

It was found that departures from full symmetry destroys spin-glass states, while retrieval states in associative memory models were found to be robust to the presence of weak asymmetry [15,39,40].

Theorists also studied fully asymmetric networks, using rate models [1], networks of binary neurons [41], and networks of spiking neurons [3]. In all these models, chaotic states were shown to be present for sufficiently strong coupling. In networks of spiking neurons, chaotic states are characterized by strongly irregular activity of the constituent neurons, with self-generated fluctuations that evolve on fast-timescales. Motivated by experimental findings, recent studies have considered synaptic connectivity matrices where bidirectionally connected pairs are overrepresented with respect to a random network. In contrast with our model, in which no structure exists beyond the level of pairs of neurons, these studies have considered structured connectivity matrices in which partial symmetry is a consequence of a larger-scale structure. References [42,43] considered a connectivity clustered into groups of highly connected neurons and demonstrated that clustered connectivity could lead to slow firing-rate dynamics generated by successive transitions between up and down states within individual clusters. An overrepresentation of bidirectional connections can also arise in networks with broad in- and out-degree distributions, which affect the dynamics and the stability of asynchronous states in such networks [44]. Other works have considered connectivities with nontrivial second-order connectivity statistics and studied the resulting network dynamics. Reference [45] analyzed how the presence of connectivity patterns involving two connections (not only bidirectionally connected pairs) affected the tendency for a neuronal network to synchronize, while [46] focused on the oscillatory activity generated by partially antisymmetric delayed interactions. Taking a completely different approach, [47] showed that maximizing the number of patterns stored in a network entails an overrepresentation of bidirectionally connected pairs of neurons, which suggests that partially symmetric connectivity may be a signature of optimal information storage.

An important ingredient in our analysis is the fact that partially symmetric interaction matrices are non-normal, i.e., they are not diagonalizable by a set of mutually orthogonal eigenvectors. The influence of non-normal connectivity on network dynamics has recently received considerable attention in the neuroscience community [35,48–52]. Particularly relevant to our study is the work by Hennequin *et al.* [35], who quantified the effects of non-normality on the amplitude of the autocorrelation function in random networks. Here we extend their results by studying the full temporal shape of the autocorrelation function and by characterizing how this shape is affected by the partial symmetry of connections.

The present work is also related to models of disordered systems and spin glasses [53]. Most studies in that field were inspired by physical phenomena and considered fully symmetric interaction matrices. In that context, a major result has been the discovery of aging, the phenomenon by which dynamics become slower the longer the system evolves [36,54,55]. This phenomenon has been observed in a broad class of complex

systems characterized by configuration spaces with extremely rugged energy landscapes, composed of many local minima surrounded by high barriers. In these systems a random initial condition is very likely to set the system far from a stationary state and initiate a very slow relaxation towards a fixed point. The relaxation takes infinitely long for $N \to \infty$ because, loosely speaking, the longer the system evolves, the deeper it wanders in the valleys of the energy landscape and the harder it becomes for it to find configurations of lower energy [36].

Whether fully symmetric interactions are necessary to observe aging does not seem to be entirely understood, as only a few works seem to have considered partially symmetric coupling [15,56,57]. Fully asymmetric networks have received more attention, but they do not exhibit any aging phenomena. Here we interpolated between fully asymmetric and fully symmetric networks and have been able to obtain mathematical results only in linear networks, in the nonchaotic regime. Interestingly, we found that the partially symmetric case is mathematically more complex than the symmetric or asymmetric limits. This can be seen in the form of the auto-correlation function (11), which simplifies considerably when $\eta = 0$ or $\eta = 1$, but also in the dynamical mean-field theory (Appendix D), where a coupling between the autocorrelation and the response function appears for $\eta > 0$. This additional complexity results from the fact that the influence of a single neuron's activity on all the other neurons is fed back through couplings that are correlated with the neuron's activity, due to the partial symmetry of the connections. More specifically, the inputs received by neuron i are given by terms $\sum_j J_{ij} \phi(x_j)$, which are themselves influenced by the activity of neuron i. As a result, neuron i influences its own activity by an amount proportional to the sum $\sum_j J_{ij} J_{ji} \phi(x_i)$, a random number of mean $\eta \phi(x_i)$. The effect of this feedback loop is that the individual input terms exhibit correlated fluctuations. When $\eta = 0$, the inputs received by neurons are uncorrelated and their sum can be approximated by a Gaussian random variable whose mean and variance can be determined self-consistently [1,19]. At the other extreme, when $\eta = 1$, the inputs received by neurons are correlated, but the dynamics of the network can be described as a relaxation of an energy function and the standard machinery of statistical mechanics can be used. For other values of η, none of these analytical strategies can be applied and the analysis becomes more complex. Demonstrating analytically whether aging dynamics is present in partially symmetric, nonlinear networks seems an outstanding open problem.

Our results on the autocorrelation function in the linear network are closely related to recent results published by Bravi *et al.* [34], who used a different set of methods to compute the power spectrum of the network activity, i.e., the Fourier transform of the autocorrelation function of the same model we investigated. Unlike Bravi *et al.* [34], we obtained the autocorrelation directly in real time, although our results are fully consistent with theirs in that we obtain the same two regimes with the same asymptotic timescales, depending on the symmetry and the gain [or leak, in their case; compare Fig. 1 of [34] with Fig. 3(a)].

Our work provides a potential bridge between two seemingly unrelated observations in neuroscience. The first is the observation of strong correlations between the synaptic strengths in pairs of cortical pyramidal cells, the main exci-

tatory neuronal type in cerebral cortex, by multiple groups using *in vitro* electrophysiological recordings [9–12]. These correlations are a consequence of two features of the connectivity. First, there exists an overrepresentation of bidirectionally connected pairs, compared to a Erdős-Rényi network with the same connection probability. For instance, Song *et al.* [10] found a connection probability of $c = 0.116$ in pairs of neurons whose somas are less than $100 \ \mu$m apart, while the probability that a pair of such neurons are connected bidirectionally is approximately $4c^2$. This degree of overrepresentation has been found in multiple cortical areas, except in the barrel cortex where no such overrepresentation exists [58]. Second, synaptic connections in bidirectionally connected pairs are on average stronger than those in unidirectionally connected pairs and are significantly correlated [10]. These observations lead to estimates of $\eta \sim 0.5$, a value that, according to our model, would lead to a significant increase in autocorrelation timescales compared to a random asymmetric connectivity.

The second observation is of long-timescales in the autocorrelations of neuronal activity from *in vivo* electrophysiological recordings (see, e.g., [18,59]). Interestingly, the timescales of these autocorrelations increase from sensory to higher level areas such as the prefrontal cortex. Several mechanisms have been proposed to account for this phenomenon: differences in the level of expression of slow N-methyl-D-aspartate (NMDA) receptors [60] or an increase in the strength of recurrent connectivity [61] which could in particular lead to the presence of multiple fixed points that can slow down the dynamics [42,43]. Our results suggest that this increase in timescale could also be due to an increase in the degree of symmetry of cortical connectivity. This would be consistent with the study of Wang *et al.* [14], who showed that the overrepresentation of bidirectionally connected pairs of neurons is significantly stronger in the prefrontal cortex than in the visual cortex.

From a neuroscience point of view, the model considered here is an extremely simplified model of cortical networks because it lacks the fundamental constraint that neurons are either excitatory or inhibitory and because it does not constrain firing rates to be positive. These simplifications were made for the sake of mathematical tractability. A few recent studies have investigated how these two constraints influence the dynamics of such networks [20–22,62–64]. Extending those works to connectivity with segregated excitation and inhibition and partial symmetry is an important direction for future work that might be facilitated by recent developments in random matrix theory [65,66].

APPENDIX A: DERIVATION OF THE DOUBLE COMPLEX INTEGRAL

We summarize here the derivation of the double complex integral of Eq. (9). Before doing so, we sketch the derivation of the local density of the overlap done in Ref. [16], as this will let us introduce some notation and pave the way for our calculation.

For a complex variable $z = x + iy$, with x and y real and with conjugate $\bar{z} = x - iy$, we define the Wirtinger derivatives $\partial/\partial z = (\partial/\partial x - i\partial/\partial y)/2$ and $\partial/\partial\bar{z} = (\partial/\partial x + i\partial/\partial y)/2$, which obey $\partial z/\partial z = \partial\bar{z}/\partial\bar{z} = 1$ as well as $\partial\bar{z}/\partial z = \partial z/\partial\bar{z} = 0$. The complex differential is defined to be $d^2z \equiv dz d\bar{z} = 2dx dy$, where the factor 2 comes from the Jacobian. We also define the complex Dirac delta so that it obeys the relation $\int \delta^2(z)d^2z \equiv 1$, which implies $\delta^2(z) = (1/2)\delta(x)\delta(y)$ given our convention for the complex differential. Two useful identities for the δ function in the complex plane are

$$\delta^2(z) = \frac{1}{2\pi}\frac{\partial}{\partial\bar{z}}\frac{1}{z} = \frac{1}{2\pi}\frac{\partial}{\partial z}\frac{1}{\bar{z}}, \tag{A1}$$

which can be checked by integrating over d^2z and applying the complex version of Green's theorem

$$\int\left(\frac{\partial v}{\partial z} + \frac{\partial\bar{v}}{\partial\bar{z}}\right)d^2z = i\oint(v\,d\bar{z} - \bar{v}\,dz), \tag{A2}$$

where v and $\bar{v}$ are to be considered independent functions.

The resolvent, defined for any matrix $\mathbf{J}$ as $(z\mathbf{1} - \mathbf{J})^{-1}$, is a key quantity in the analysis of random matrices because it can be ensemble averaged using standard methods and can be related to quantities of interest. So, for example, the empirical density of eigenvalues of a given $\mathbf{J}$,

$$\rho_J(z) = \frac{1}{N}\sum_{i=1}^{N}\delta(x - \mathrm{Re}\,\lambda_i)\delta(y - \mathrm{Im}\,\lambda_i) = \frac{2}{N}\sum_{i=1}^{N}\delta^2(z - \lambda_i),$$

can be expressed due to the identities (A1) as

$$\rho_J(z) = \frac{1}{\pi}\frac{\partial}{\partial\bar{z}}\frac{1}{N}\sum_{i=1}^{N}\frac{1}{z - \lambda_i} = \frac{1}{\pi}\frac{\partial}{\partial\bar{z}}\frac{1}{N}\,\mathrm{Tr}(z\mathbf{1} - \mathbf{J})^{-1}.$$

This quantity is hard to compute for any particular realization at finite N, but it becomes easier to handle in the limit of large N, where all empirical densities converge to the average density

$$\rho(z) = [\rho_J(z)]_J = \frac{1}{\pi}\frac{\partial}{\partial\bar{z}}\left[\frac{1}{N}\,\mathrm{Tr}(z\mathbf{1} - \mathbf{J})^{-1}\right]_J.$$

Deriving the average density, therefore, amounts to computing the function $G(z) = [\mathrm{Tr}(z\mathbf{1} - \mathbf{J})^{-1}/N]_J$ in the large-N limit.

The local density of the overlap can be derived in a similar manner using the spectral decomposition $(z\mathbf{1} - \mathbf{J})^{-1} = \sum_{i=1}^{N}\mathbf{R}_i(z - \lambda_i)^{-1}\mathbf{L}_i^\dagger$, where $\mathbf{R}_i$ and $\mathbf{L}_i$ are the right and left eigenvectors of $\mathbf{J}$, respectively. If we substitute the definition of the overlap matrix into Eq. (8) and use the identities (A1) we obtain

$$D(z_1, z_2)$$

$$= \frac{4}{N}\left[\sum_{i,j=1}^{N}(\mathbf{L}^\dagger\mathbf{L})_{ij}(\mathbf{R}^\dagger\mathbf{R})_{ji}\delta^2(z_1 - \lambda_i)\delta^2(z_2 - \lambda_j)\right]_J$$

$$= \frac{1}{N\pi^2}\frac{\partial}{\partial\bar{z}_1}\frac{\partial}{\partial z_2}\left[\sum_{i,j=1}^{N}\mathrm{Tr}\,\mathbf{R}_i\frac{1}{z_1 - \lambda_i}\mathbf{L}_i^\dagger\mathbf{L}_j\frac{1}{\bar{z}_2 - \bar{\lambda}_j}\mathbf{R}_j^\dagger\right]_J$$

$$= \frac{1}{\pi^2}\frac{\partial}{\partial\bar{z}_1}\frac{\partial}{\partial z_2}\left[\frac{1}{N}\,\mathrm{Tr}\,\frac{1}{z_1\mathbf{1} - \mathbf{J}}\frac{1}{\bar{z}_2\mathbf{1} - \mathbf{J}^\dagger}\right]_J \tag{A3}$$

and the problem reduces to computing the quantity

$$G(z_1, z_2) = \left[\frac{1}{N}\,\mathrm{Tr}\,\frac{1}{z_1\mathbf{1} - \mathbf{J}}\frac{1}{\bar{z}_2\mathbf{1} - \mathbf{J}^\dagger}\right]_J.$$

The expression of $G(z_1, z_2)$ for the ensemble of Gaussian random matrices with partial symmetry was derived by Mehlig and Chalker [17]. The basic idea behind their calculation is to expand resolvents in power series, average over the disorder term by term, and organize the sums so that a recursive relation can be established and ultimately solved (for a thorough description of the method, see also [52]). The result is a complex function that takes the value

$$G(z_1, z_2)$$

$$= \frac{1}{1 - \eta^2}\left(\frac{(1 - \eta^2)^2 + \eta(z_1^2 + \bar{z}_2^2) - (1 + \eta^2)z_1\bar{z}_2}{|z_1 - z_2|^2} - 1\right), \tag{A4}$$

when both z_1 and z_2 lie inside the ellipse centered at the origin and which has major and minor radii $1 + \eta$ and $1 - \eta$, respectively. We will call this ellipse E_η for later convenience. When z_1 and z_2 lie outside E_η we have instead

$$G(z_1, z_2) = \frac{h_1\bar{h}_2}{1 - h_1\bar{h}_2},$$

where

$$h_1 = \frac{z_1 - \sqrt{z_1^2 - 4\eta}}{2\eta}, \quad \bar{h}_2 = \frac{\bar{z}_2 - \sqrt{\bar{z}_2^2 - 4\eta}}{2\eta}.$$

Right on the ellipse E_η, $|h_i| = 1$. When both z_1 and $\bar{z}_2$ lie outside the ellipse, the function $G(z_1, z_2)$ is analytic on z_1 and $\bar{z}_2$. This analyticity implies, from (A3), that the local density of the overlap vanishes outside the ellipse.

We now proceed to compute $A(u, \tau)$ [Eq. (10)]. Inserting the identity (A3) into (10) leads to

$$A(u, \tau) = \frac{1}{4\pi^2}\iint e^{g(z_1 + \bar{z}_2)u + gz_1\tau}\frac{\partial}{\partial\bar{z}_1}\frac{\partial}{\partial z_2}G(z_1, z_2)d^2z_1 d^2z_2.$$

Because the exponential prefactor is analytic in z_1 and $\bar{z}_2$, it commutes with the two partial derivatives. We can therefore apply Green's theorem twice to obtain

$$A(u, \tau) = \frac{1}{4\pi^2}\oint_E\oint_E e^{g(z_1 + \bar{z}_2)u + gz_1\tau}G(z_1, z_2)dz_1 d\bar{z}_2, \tag{A5}$$

where both contour integrals are around the ellipse E, at whose boundary $G(z_1, z_2)$ stops being analytic. To compute $A(u, \tau)$ we follow the approach of [17] and use the linear transformation $w = (z - \eta\bar{z})/(1 - \eta^2)$ (or, equivalently, $z = w + \eta\bar{w}$) to reshape the contour of integration from the ellipse E_η into the unit circle. Applying this transformation to both z_1 and z_2, the surface integrals in Eq. (A5) become contour integrals on the unit circle $|w|^2 = w\bar{w} = 1$. On this contour we
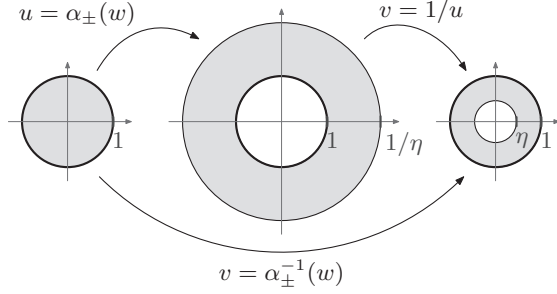
FIG. 6. Mapping of the unit disk $D = \{w \in \mathbf{C} \mid |w| \leqslant 1\}$ by the functions $\alpha_\pm(w)$ and $\alpha_\pm^{-1}(w)$.

can replace every $\bar{w}$ in the integrand by w^{-1} and we can use the standard tools of complex analysis to carry out the integrals. We describe in more detail our derivation in the following.

We start by performing the integral over $\bar{z}_2$, expressing Eq. (A4) in terms of w_1, $\bar{w}_1$, and w_2, and replacing all $\bar{w}_2$ by w_2^{-1}. After some simplifications, we obtain

$$
\begin{aligned}
&G(z_1(w_1), z_2(w_2)) \\
&= -1 + \frac{1}{\eta(\alpha_+ - \alpha_-)}\left(\frac{1 - \eta w_1 \alpha_+}{w_2 - \alpha_+} - \frac{1 - \eta w_1 \alpha_-}{w_2 - \alpha_-}\right),
\end{aligned}
\tag{A6}
$$

where we defined the poles

$$
\alpha_\pm(w_1) = \frac{\bar{w}_1 + \eta w_1 \pm \sqrt{(\bar{w}_1 + \eta w_1)^2 - 4\eta}}{2\eta}.
\tag{A7}
$$

These poles depend on w_1 and can be shown to map the unit disk onto an annulus of inner radius 1 and outer radius $1/|\eta|$ (see Fig. 6). This information will be relevant when we use residue calculus.

The double integral (A5) has to be regularized because the integrand diverges at $z_1 = z_2$. Our regularization consists of first integrating w_2 on the unit circle while constraining w_1 to be on a concentric circle of smaller radius $|w_1| = 1 - \epsilon$, with $\epsilon > 0$ small. Once the integral over w_2 is done, we take the limit $\epsilon \to 0$ and perform the second integral over w_1.

Under this regularization, we decompose the double integral (A5) as

$$
\begin{aligned}
A(u, \tau) = \lim_{\epsilon \to 0} \frac{1}{4\pi^2} &\oint_{|w_1| = 1-\epsilon} e^{g(w_1 + \eta \bar{w}_1)(u+\tau)} \mathcal{A}(w_1, u) \\
&\times (dw_1 + \eta d\bar{w}_1),
\end{aligned}
\tag{A8}
$$

where we used $z_1 = w_1 + \eta \bar{w}_1$ and defined

$$
\begin{aligned}
\mathcal{A}(w_1, u) = &\oint_{|w_2| = 1} e^{g(w_2^{-1} + \eta w_2)u} G(z_1(w_1), z_2(w_2)) \\
&\times \left(-\frac{1}{w_2^2} + \eta\right) dw_2.
\end{aligned}
\tag{A9}
$$

Note that here we used $\bar{w}_2 = w_2^{-1}$ to express the integrand and the differential $d\bar{z}_2 = d\bar{w}_2 + \eta dw_2$ in terms of w_2 only. The integrand of Eq. (A9) contains one singularity inside the contour of integration, at $w_2 = 0$. This singularity is associated with the essential singularity from the exponential e^{1/w_2} as well as with the pole of second order $1/w_2^2$. Because we are

assuming that $|w_1| < 1$, the poles of $G(z_1(w_1), z_2(w_2))$ at $w_2 = \alpha_\pm$ lie outside the contour and therefore do not contribute to the integral. We are thus left with the task of computing the residue at the origin. We do that by expanding the integrand in Laurent series around $w_2 = 0$, using the relations

$$
e^{(z^{-1} + \eta z)t} = \sum_{k=-\infty}^{\infty} (z\sqrt{\eta})^k I_k(2\sqrt{\eta}t) \quad \text{for } z \neq 0,
$$

$$
(z - z_0)^{-1} = -\frac{1}{z_0} \sum_{k=0}^{\infty} \left(\frac{z}{z_0}\right)^k \quad \text{for } |z| < |z_0|,
$$

with $I_k(z)$ being the modified Bessel function of order k. We use the last power series to expand the terms $(w_2 - \alpha_\pm)^{-1}$ in $G(z_1(w_1), z_2(w_2))$ [Eq. (A6)]. This power series converges because $|w_2| < |\alpha_\pm|$ when $|w_1| < 1$, as we assume in our regularization scheme. After expanding, applying Cauchy's residue theorem, and taking the limit $\epsilon \to 0$, we obtain

$$
\mathcal{A}(w_1, u) = -\frac{2\pi i}{gu} \sum_{k=0}^{\infty} w_1^{-k} \eta^{-k/2} k I_k(2g\sqrt{\eta}u).
$$

The final step is to compute the integral in Eq. (A8) with the same strategy we used for $\mathcal{A}(w_1, u, \tau)$. In this case we express the integrand in terms of w_1 only and we expand the exponential factor in Eq. (A8) with the identity

$$
e^{(z + \eta z^{-1})t} = \sum_{k=-\infty}^{\infty} \left(\frac{z}{\sqrt{\eta}}\right)^k I_k(2\sqrt{\eta}t).
$$

We then pick the residue from the expansion and apply Cauchy's theorem. The result is

$$
A(u, \tau) = A_1(u, \tau) + A_2(u, \tau),
$$

with

$$
\begin{aligned}
A_1(u, \tau) = \sum_{k=-\infty}^{\infty} &\eta^{k/2} I_k(2g\sqrt{\eta}\tau)[(1 + \eta^2) I_k(2g(1+\eta)u) \\
&- \eta(I_{k-2}(2g(1+\eta)u) + I_{k+2}(2g(1+\eta)u))]
\end{aligned}
\tag{A10}
$$

and $A_2(u, \tau)$ given by Eq. (13).

The expression (A10) for $A_1(u, \tau)$ can be further simplified with the identity [67]

$$
\begin{aligned}
&\sum_{k=-\infty}^{\infty} e^{ik\alpha} J_k(w) J_{k+\nu}(z) \\
&= \left(\frac{z - we^{-i\alpha}}{z - we^{i\alpha}}\right)^{\nu/2} J_\nu(\sqrt{w^2 + z^2 - 2wz\cos\alpha}),
\end{aligned}
\tag{A11}
$$

which we can transform into a more convenient expression for our problem, using $J_\nu(iz) = i^\nu I_\nu(z)$ and taking $\alpha = \pi - (i/2)\ln\eta$ so that $e^{i\alpha} = -\sqrt{\eta}$. The identity (A11) then becomes

$$
\begin{aligned}
&\sum_{k=-\infty}^{\infty} \eta^{k/2} I_k(w) I_{k+\nu}(z) \\
&= \left(\frac{z + w\eta^{-1/2}}{z + w\eta^{1/2}}\right)^{\nu/2} I_\nu(\sqrt{w^2 + z^2 + wz(\eta^{1/2} + \eta^{-1/2})}),
\end{aligned}
\tag{A12}
$$

which allows us to rewrite Eq. (A10) as the final expression (12).

The series $A_2(u,\tau)$ does not seem to have a closed expression for general η. For $\eta = 1$, however, we can exploit the identity

$$\sum_{k=-\infty}^{\infty} I_k(w) I_{n-k}(z) = I_n(w+z)$$

to conclude that

$$A_2(u,\tau) = -I_0(2g(2u+\tau)) + I_2(2g(2u+\tau)) \quad \text{for } \eta = 1.$$

APPENDIX B: EVALUATION OF THE TIME INTEGRAL FOR LONG τ

The exact average autocorrelation is given in Eq. (9) as a time integral that can be decomposed as

$$C(\tau) = \int_0^\infty e^{-2u-\tau} [A_1(u,\tau) + A_2(u,\tau)] du,$$

where $A_1(u,\tau)$ and $A_2(u,\tau)$ are defined in Eqs. (12) and (13). To gain more analytical insight we will evaluate $C(\tau)$ when τ is sufficiently large, a limit that allows us to invoke Laplace's method and approximate the integral with a closed-form expression [68]. Before applying the limit it is convenient to express this integral in terms of a new variable $\xi \equiv u/\tau$, which is well defined for $\tau > 0$. With this definition

$$C(\tau) = \int_0^\infty e^{-\tau(2\xi+1)} [A_1(u(\xi),\tau) + A_2(u(\xi),\tau)] \tau \, d\xi$$
$$\equiv C_1(\tau) + C_2(\tau), \tag{B1}$$

which we split into the two terms composing the integrand. We start with the asymptotic dependence of $C_1(\tau)$, ignoring for the moment $C_2(\tau)$. The integrand of $C_1(\tau)$ contains $I_0(\cdot)$ and $I_2(\cdot)$, whose argument is large in the long-τ limit. We can therefore use the asymptotic expansion of the modified Bessel functions of order ν,

$$I_\nu(x) = \frac{e^x}{\sqrt{2\pi x}} \left[1 - \frac{4\nu^2 - 1}{8x} + O(x^{-2}) \right] \quad \text{for } x \gg 1. \tag{B2}$$

At this order, defining

$$\psi(\xi;\eta) \equiv \psi(u(\xi),\tau;\eta)/\tau = 2\sqrt{(1+\eta)^2 \xi(\xi+1) + \eta},$$

we obtain

$$C_1(\tau) = \sqrt{\frac{\tau}{2\pi}} \int_0^\infty \frac{\exp\{-\tau[(2\xi+1) - g\psi(\xi;\eta)]\}}{\sqrt{g\psi(\xi;\eta)}}$$
$$\times \left[(1+\eta^2)\left(1 + \frac{1}{8\tau g\psi(\xi;\eta)}\right) \right.$$
$$\left. - 2\eta\left(1 + \frac{2(1-\eta)^2}{\psi(\xi;\eta)^2}\right)\left(1 - \frac{15}{8\tau g\psi(\xi;\eta)}\right) \right] d\xi, \tag{B3}$$

with $g = (1-\delta)/(1+\eta)$. This integral is of the form

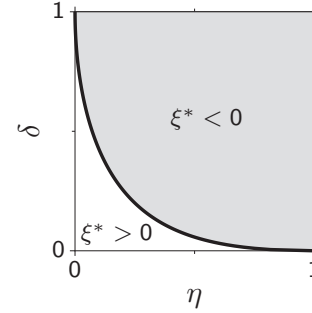$$A(\tau) = \int_0^\infty f(\xi) e^{\tau b(\xi)} d\xi. \tag{B4}$$

FIG. 7. Sign of ξ^*, at which the exponent in Eq. (B3) is largest, as a function of the spectral gap and the degree of symmetry. This diagram is equivalent to that shown in Fig. 3(a), after transforming δ into its associated gain $g = (1-\delta)/(1+\eta)$.

In the limit of large τ, only the infinitesimal interval around the maximum of $b(\xi)$ contributes to the integral because the contribution of the remaining intervals is exponentially suppressed. In our particular case the maximum of $b(\xi)$ is at

$$\xi^* = \frac{1}{2}\left(-1 + \frac{1-\eta}{(1+\eta)\sqrt{2\delta - \delta^2}} \right). \tag{B5}$$

We distinguish two cases. For large enough values of η and δ, ξ^* is negative (Fig. 7), which means that in the integration range $[0,\infty)$ of Eq. (B3) the maximum value of $b(\xi)$ is at $\xi = 0$. Conversely, for low values of η and δ, the maximum of $b(\xi)$ occurs within $(0,\infty)$. These two cases will lead to different time dependences and will be studied separately in the following.

For values of η and δ such that $\xi^* < 0$, the limit $\tau \to \infty$ of Eq. (B4) can be approximated by (see [68], pp. 266–268)

$$A(\tau) \sim \lim_{\epsilon \to 0} \int_0^\epsilon f(0) e^{\tau[b(0)+b'(0)s]} ds$$
$$\sim \int_0^\infty f(0) e^{\tau[b(0)+b'(0)s]} ds \sim -\frac{f(0)e^{\tau b(0)}}{\tau b'(0)}, \tag{B6}$$

where $b'(0)$ denotes the derivative of $b(\xi)$ evaluated at $\xi^* = 0$. Applying this approximation to (B3), we obtain

$$C_1(\tau) = \frac{\tau^{-3/2}\eta^{-1/4}}{2\sqrt{\pi}} \frac{1+\eta^2}{\delta(1+\eta) - [1-\sqrt{\eta}]^2} \left(\frac{1+\eta}{1-\delta}\right)^{3/2}$$
$$\times \exp\left\{ -\tau \frac{(1-\sqrt{\eta})^2 + 2\delta\sqrt{\eta}}{1+\eta} \right\}. \tag{B7}$$

Conversely, if η and δ are such that $\xi^* > 0$, the maximum ξ^* falls within the integration region and we can approximate the large-τ limit of the integral (B4) by (see [68], p. 267)

$$A(\tau) \sim \lim_{\epsilon \to 0} \int_{\xi^*-\epsilon}^{\xi^*+\epsilon} f(\xi^*) e^{\tau[b(\xi^*)+(s-\xi^*)^2 b''(\xi^*)/2]} ds$$
$$\sim \int_{-\infty}^\infty f(\xi^*) e^{\tau[b(\xi^*)+(s-\xi^*)^2 b''(\xi^*)/2]} ds$$
$$\sim \frac{\sqrt{2\pi} f(\xi^*) e^{\tau b(\xi^*)}}{\sqrt{-\tau b''(\xi^*)}},$$

with $b''(\xi^*)$ denoting the second derivative of $b(\xi)$ evaluated at ξ^*. In this case Eq. (B3) is approximately given by

$$C_1(\tau) = \frac{\delta^{-1/2}(1-\eta)^2}{2\sqrt{2}(1-\delta)} \exp\left\{-\tau \frac{1-\eta}{1+\eta}\sqrt{2\delta-\delta^2}\right\}.$$

We now turn to the asymptotic dependence of $C_2(\tau)$. The original form for $C_2(\tau)$ is

$$C_2(\tau) = \int_0^\infty \left\{ e^{-\tau(2\xi+1)} \sum_{k=0}^\infty \eta^{k+2}(k+1)^2 \right.$$
$$\left. \times \frac{I_{k+1}(2g\tau\sqrt{\eta}\xi)I_{k+1}(2g\tau\sqrt{\eta}(\xi+1))}{\eta\tau g^2\xi(\xi+1)} \right\}d\xi.$$
$$(B8)$$

The integrand contains a product of Bessel functions that grows exponentially with τ [see Eq. (B2)], but this growth is kept in check by the exponential prefactor. To see this, we introduce the scaled modified Bessel function

$$I_\nu^*(x) \equiv e^{-x}I_\nu(x)$$

in terms of which (B8) becomes

$$C_2(\tau) = \int_0^\infty \exp\left[-\tau \frac{(1-\sqrt{\eta})^2 + 2\delta\sqrt{\eta}}{1+\eta}\right] \sum_{k=0}^\infty \eta^{k+1}(k+1)^2$$
$$\times \frac{I_{k+1}^*(2g\tau\sqrt{\eta}\xi)I_{k+1}^*(2g\tau\sqrt{\eta}(\xi+1))}{\tau g^2\xi(\xi+1)}d\xi. \quad (B9)$$

The integral converges because the exponential decays to zero for large τ and trumps the power-law decay of $I_k^*(\cdot)$. Equation (B9) also has the same form as (B4) and contains exactly the same exponent as in Eq. (B7); because the exponential attains its maximum at $\xi = 0$, we can use the approximation (B6). To evaluate at $\xi = 0$ we use the power expansion $I_{k+1}^*(2g\tau\sqrt{\eta}\xi) \overset{\xi\sim0}{=} (g\tau\sqrt{\eta}\xi)^{k+1}$ and identify $f(\xi)$ in Eq. (B6) with

$$f(\xi) \equiv \sum_{k=0}^\infty \frac{\eta^{3(k+1)/2}}{\xi+1}(k+1)^2 g^{k-1}\xi^k\tau^k I_{k+1}^*(2g\tau\sqrt{\eta}(\xi+1)).$$

All the terms of $f(\xi)$ with $k > 0$ vanish at $\xi = 0$ and Eq. (B6) reads in this case

$$C_2(\tau) \sim \frac{\tau^{-3/2}\eta^{5/6}}{4\sqrt{\pi}} \frac{(1+\eta)^{5/2}}{(1-\delta)^{3/2}} \frac{1}{(1-\sqrt{\eta})^2 + 2\sqrt{\eta}\delta}$$
$$\times \exp\left\{-\tau \frac{(1-\sqrt{\eta})^2 + 2\delta\sqrt{\eta}}{1+\eta}\right\}.$$

Summing this contribution to that in Eq. (B7) leads to the result reported in Eqs. (18)–(20).

APPENDIX C: AUTOCORRELATION WITHOUT OVERLAPS

Here we compute the autocorrelation ignoring the effect of the overlaps between eigenvectors. In this case, we need to compute the individual contribution of a sratingle eigenvalue to the autocorrelation and then sum over the contributions of

all eigenvalues. We start with the one-dimensional version of Eq. (4),

$$\frac{dx}{dt} = \alpha x + \sigma\xi(t), \quad (C1)$$

where the parameter α would be the (single) eigenvalue of the system, assumed to have a negative real part to prevent $x(t)$ to grow unbounded, and where $\xi(t)$ is a source of standard Gaussian white noise. The solution of (C1) is

$$x(t) = \sigma \int_{-\infty}^t e^{\alpha(t-s)}\xi(s)ds,$$

from which we can derive the autocorrelation

$$\langle x(t)x(t+\tau)\rangle = \sigma^2 \int_{-\infty}^t \int_{-\infty}^{t+\tau} e^{\alpha(2t+\tau-s-u)}\langle\xi(s)\xi(u)\rangle ds\,du$$
$$= -\sigma^2 \frac{e^{\alpha\tau}}{2\alpha} \equiv \sigma^2 C_\alpha(\tau). \quad (C2)$$

The eigenvalue α determines both the timescale and the amplitude of the autocorrelation. We set the overall factor σ^2 to 1, without loss of generality.

The average autocorrelation for the high-dimensional system in the absence of overlaps is the sum of (C2) over all the eigenvalues. In the large-N limit we would have

$$C(\tau) = \frac{1}{N} \sum_{i=1}^N C_{\alpha_i}(\tau) \xrightarrow{N\to\infty} \int C_\alpha(\tau)\rho(\alpha)d\alpha\,d\bar{\alpha}, \quad (C3)$$

where $\rho(\alpha)$ is the probability density of eigenvalues and the integral is on the complex plane. For the system (4) and for the connectivity matrices we consider, the density of the eigenvalues α is uniform and has support on an ellipse centered at $z = -1$ with major radius $g(1+\eta)$ and minor radius $g(1-\eta)$. The integral (C3) can be computed in that case and reads

$$C(\tau) = \frac{-1}{\pi g^2(1-\eta^2)} \int_E \frac{e^{\alpha\tau}}{2\alpha}d\alpha\,d\bar{\alpha}, \quad (C4)$$

where we used Eq. (C2) and the prefactor is the constant value that $\rho(\alpha)$ takes on the elliptic support E. To evaluate the integral we use the parametrization

$$\alpha = -1 + r(1+\eta)\cos\theta + ir(1-\eta)\sin\theta$$

and integrate over $r \in [0,g]$ and $\theta \in [0,2\pi]$. Noting that

$$\int_E d\alpha\,d\bar{\alpha} = (1-\eta^2) \int_0^{2\pi} \int_0^g r\,dr\,d\theta,$$

Eq. (C4) becomes

$$C(\tau) = \frac{1}{\pi g^2} \int_0^{2\pi} \int_0^g \frac{\exp\{-\tau[1 - r\psi(\theta)]\}}{2[1 - r\psi(\theta)]}r\,dr\,d\theta, \quad (C5)$$

where for convenience we defined

$$\psi(\theta) \equiv (1+\eta)\cos\theta + i(1-\eta)\sin\theta.$$

The integral (C5) is hard to compute, but we can make progress by taking the derivative of $C(\tau)$ with respect to τ,

$$C'(\tau) = -\frac{e^{-\tau}}{2\pi g^2} \int_0^{2\pi} \int_0^g e^{\tau \psi(\theta) r} r \, dr \, d\theta, \qquad \text{(C6)}$$

which is easier to evaluate. Equation (C6) can be integrated over r by parts, yielding an integral over θ only that, excluding prefactors, reads

$$B(g,\tau) \equiv \int_0^{2\pi} \left\{ \frac{g e^{\tau \psi(\theta) g}}{\tau \psi(\theta)} - \frac{e^{\tau \psi(\theta) g} - 1}{\tau^2 \psi^2(\theta)} \right\} d\theta.$$

Again, this integral is hard to compute but we can use the same trick we used before, noting that the partial derivative of $A(g,\tau)$ with respect to g simplifies considerably,

$$\frac{\partial B(g,\tau)}{\partial g} = g \int_0^{2\pi} e^{\tau \psi(\theta) g} d\theta = 2\pi g I_0(2g\tau\sqrt{\eta}),$$

where in the last equation we used Eq. (3.937.2) in Ref. [69]. We recover the expression for $A(g,\tau)$ by integrating along g, with the initial condition $A(0,\tau) = 0$:

$$B(g,\tau) = 2\pi \int_0^g x I_0(2x\tau\sqrt{\eta}) dx = \frac{2\pi}{4\tau^2\eta} \int_0^{2g\tau\sqrt{\eta}} y I_0(y) dy.$$

The last integral can be computed with the help of the recurrence relation $z I_0(z) = z I_1'(z) + I_1(z)$. An integration by parts of the term $z I_1'(z)$ leads to the final identity $\int x I_0(x) dx = x I_1(x)$ and therefore to

$$B(g,\tau) = \frac{\pi g}{\tau \sqrt{\eta}} I_1(2\tau g \sqrt{\eta}).$$

Equation (C6) then reads

$$C'(\tau) = -\frac{e^{-\tau}}{2\tau g \sqrt{\eta}} I_1(2\tau g \sqrt{\eta}), \qquad \text{(C7)}$$

which we have to integrate to recover $C(\tau)$. Such an integration is subject to the initial condition $C(0)$,

$$C(0) = \frac{1}{2\pi g^2} \int_0^{2\pi} \int_0^g \frac{r}{1 - r\psi(\theta)} dr \, d\theta$$

$$= -\frac{1}{2\pi g^2} \int_0^{2\pi} \left\{ \frac{g}{\psi(\theta)} + \frac{1}{\psi^2(\theta)} \ln[1 - g\psi(\theta)] \right\} d\theta,$$

which can be evaluated numerically.

APPENDIX D: SUMMARY OF THE DYNAMIC MEAN-FIELD DERIVATION

The starting point of the calculation is the moment generating functional for the state variables $x_i(t)$ obeying Eq. (1). We consider the more general case where the activation variable is driven by recurrent inputs as well as independent external white noise

$$\dot{x}_i(t) = -x_i(t) + g \sum_{j=1}^N J_{ij} r_j(t) + \sigma \xi_i(t), \quad i = 1, \ldots, N,$$
$$\text{(D1)}$$

where we defined $r_j(t) \equiv \phi(x_j(t))$ to simplify the notation. The white-noise sources $\xi_i(t)$ have zero mean and unit variance.

The moment generating functional for such a system can be shown to be [70,71] (see also [72,73] for a more pedagogical description)

$$Z[l,\tilde{l};\mathbf{J}] = \int \mathcal{D}x(t)\mathcal{D}\tilde{x}(t) \exp\left(-S[x,\tilde{x};\mathbf{J}] \right.$$

$$\left. + \sum_{i=1}^N \int \tilde{l}_i(t) x_i(t) dt + \sum_{i=1}^N \int l_i(t) \tilde{x}_i(t) dt \right),$$

where $\mathcal{D}x(t)\mathcal{D}\tilde{x}(t) = \prod_{i=1}^N \mathcal{D}x_i(t)\mathcal{D}\tilde{x}_i(t)$ is the functional measure for all possible paths for all variables and we introduced the action

$$S[x,\tilde{x};\mathbf{J}]$$
$$= \sum_{i=1}^N \int \tilde{x}_i(t) \left\{ \dot{x}_i(t) + x_i(t) - g \sum_{j=1}^N J_{ij} r_j(t) - \frac{\sigma^2}{2} \tilde{x}_i(t) \right\} dt.$$
$$\text{(D2)}$$

In this definition we assume that the auxiliary fields $\tilde{x}(t)$ are purely imaginary, so we do not have to write explicit imaginary units all along. By construction the generating functional satisfies the normalization condition $Z[0,0;\mathbf{J}] = 1$. The fact that $Z[0,0;\mathbf{J}]$ does not depend on $\mathbf{J}$ allows us to compute the quenched average directly on Z [74],

$$Z[l,\tilde{l}] \equiv \int \frac{Z[l,\tilde{l};\mathbf{J}]}{Z[0,0;\mathbf{J}]} dP(\mathbf{J}) = \int Z[l,\tilde{l};\mathbf{J}] dP(\mathbf{J}), \quad \text{(D3)}$$

which simplifies considerably the average, now reduced to computing $[\exp(-S[x,\tilde{x},\mathbf{J}])]_J$. To do so, we use the decomposition of partially symmetric connectivity matrices

$$J_{ij} = J_{ij}^s + k J_{ij}^a, \qquad \text{(D4)}$$

where $J_{ij}^s = J_{ji}^s$, $J_{ij}^a = -J_{ji}^a$, and both J_{ij}^s and J_{ij}^a are Gaussian random variates with zero mean and variance

$$\left[(J_{ij}^s)^2 \right]_J = \left[(J_{ij}^a)^2 \right]_J = \frac{1}{N} \frac{1}{1+k^2}$$

so that $[J_{ij}^2]_J = J^2/N$. With these matrix decompositions, the correlation between bidirectional weights is [15]

$$[J_{ij} J_{ji}]_J = \frac{1}{N} \frac{1-k^2}{1+k^2},$$

which must equal η/N by our definition of η. This leads to the relation $k^2 = (1-\eta)/(1+\eta)$. To integrate over the disorder we use the Gaussian measures

$$dP(\mathbf{J}^s) = \prod_{i \leqslant j} dP(J_{ij}^s) \propto \exp\left\{ -\frac{N}{1+\eta} \sum_{i \leqslant j} (J_{ij}^s)^2 \right\} d\mathbf{J}^s,$$

$$dP(\mathbf{J}^a) = \prod_{i < j} dP(J_{ij}^a) \propto \exp\left\{ -\frac{N}{1+\eta} \sum_{i < j} (J_{ij}^a)^2 \right\} d\mathbf{J}^s,$$

with $d\mathbf{J}^s = \prod_{i \leqslant j} dJ_{ij}^s$ and $d\mathbf{J}^s = \prod_{i < j} dJ_{ij}^a$. We will ignore the contribution of diagonal elements of the synaptic matrix because it is negligible in the limit of large N. We can now integrate out the terms linear in J_{ij} that appear in Eq. (D2), by separating symmetric and antisymmetric components. Excluding prefactors and time integrals, these terms are of

the form

$$
\begin{aligned}
L(\mathbf{J},t) &\equiv \sum_{\substack{i,j \\ i \neq j}} \tilde{x}_i(t) J_{ij} r_j(t) \\
&= \sum_{\substack{i,j \\ i \neq j}} \tilde{x}_i(t) \big[J_{ij}^s + k J_{ij}^a \big] r_j(t) \\
&= \sum_{i<j} \big\{ J_{ij}^s [\tilde{x}_i(t) r_j(t) + \tilde{x}_j(t) r_i(t)] + k J_{ij}^a [\tilde{x}_i(t) r_j(t) - \tilde{x}_j(t) r_i(t)] \big\}
\end{aligned}
$$

so that

$$
\int \exp\left\{ g \int L(\mathbf{J},t)dt \right\} dP(\mathbf{J}^s) dP(\mathbf{J}^a) = \exp\left\{ \frac{g^2}{2N} \sum_{\substack{i,j \\ i \neq j}} \iint \{ [\tilde{x}_i(t) r_j(t) \tilde{x}_i(t') r_j(t')] + \eta[\tilde{x}_i(t) r_j(t) \tilde{x}_j(t') r_i(t')] \} dt\, dt' \right\},
$$

where we used the property that, for a Gaussian variable z of zero mean and variance σ^2, the expected value of $\exp(\lambda z)$ is $\langle \exp(\lambda z) \rangle_z = \exp(\lambda^2 \sigma^2/2)$, which can be checked by completing the square in the exponential.

Putting back together all the pieces, the average generating functional (D3) is therefore

$$
\begin{aligned}
Z[l,\tilde{l}] = \int \mathcal{D}x(t)\mathcal{D}\tilde{x}(t) \exp\Bigg(&-S_0[x(t),\tilde{x}(t)] + \frac{\sigma^2}{2}\tilde{x}\cdot\tilde{x} + \tilde{l}\cdot x_i + l\cdot\tilde{x} \\
&+ \frac{g^2}{2N} \sum_{\substack{i,j \\ i \neq j}} \iint \{ [\tilde{x}_i(t) r_j(t) \tilde{x}_i(t') r_j(t')] + \eta[\tilde{x}_i(t) r_j(t) \tilde{x}_j(t') r_i(t')] \} dt\, dt' \Bigg),
\end{aligned} \tag{D5}
$$

where we defined the free action

$$
S_0[x,\tilde{x}] \equiv \sum_{i=1}^N \int \tilde{x}_i(t)[\dot{x}_i(t) + x_i(t)]dt \tag{D6}
$$

and we introduced the notation

$$
f \cdot g \equiv \sum_{i=1}^N \int f_i(t) g_i(t) dt.
$$

As a result of averaging out the disorder, we obtained a coupling involving four fields with different indices and at different times. To proceed, it is convenient to introduce auxiliary fields that involve terms local in space (i.e., with the same index) but not in time,

$$
q_1(t,t') = \frac{g^2}{N} \sum_{i=1}^N \tilde{x}_i(t)\tilde{x}_i(t'), \quad q_2(t,t') = \frac{g^2}{N} \sum_{i=1}^N r_i(t) r_i(t'),
$$

$$
q_3(t,t') = \frac{g^2}{N} \sum_{i=1}^N \tilde{x}_i(t) r_i(t'), \quad q_4(t,t') = \frac{g^2}{N} \sum_{i=1}^N r_i(t)\tilde{x}_i(t'),
$$

so Eq. (D5) now reads

$$
\begin{aligned}
Z[l,\tilde{l}] = \int \mathcal{D}x(t)\mathcal{D}\tilde{x}(t) &\left(\prod_{\alpha=1}^4 \frac{N}{g^2}\mathcal{D}q_\alpha \right) \delta\left(\frac{N}{g^2}q_1 - \sum_{i=1}^N \tilde{x}_i(t)\tilde{x}_i(t') \right) \delta\left(\frac{N}{g^2}q_2 - \sum_{i=1}^N r_i(t) r_i(t') \right) \delta \\
&\times \left(\frac{N}{g^2}q_3 - \sum_{i=1}^N \tilde{x}_i(t) r_i(t') \right) \delta\left(\frac{N}{g^2}q_4 - \sum_{i=1}^N r_i(t)\tilde{x}_i(t') \right) \\
&\times \exp\left(-S_0[x,\tilde{x}] + \frac{\sigma^2}{2}\tilde{x}\cdot\tilde{x} + \tilde{l}\cdot x_i + l\cdot\tilde{x} + \frac{N}{2g^2} \iint \{q_1(t,t')q_2(t,t') + \eta q_3(t,t') q_4(t,t')\} dt\, dt' \right).
\end{aligned} \tag{D7}
$$

We now express the Dirac functionals in their integral representation. The first Dirac functional appearing in Eq. (D7) can be written as

$$\delta\left(\frac{N}{g^2}q_1 - \sum_{i=1}^{N}\tilde{x}_i(t)\tilde{x}_i(t')\right) = \frac{1}{2\pi}\int \mathcal{D}\hat{q}_1(t,t')\exp\left\{\iint \hat{q}_1(t,t')\left[\frac{N}{g^2}q_1(t,t') - \sum_{i=1}^{N}\tilde{x}_i(t)\tilde{x}_i(t')\right]dt\,dt'\right\},$$

where the integral over $\hat{q}$ is understood to be along the imaginary axis. The other Dirac functionals in Eq. (D7) are rewritten analogously. Equation (D7) then becomes

$$Z[l,\tilde{l}] = \int \mathcal{D}X\mathcal{D}Q\exp\left(-S_0[x,\tilde{x}] + \frac{\sigma^2}{2}\tilde{x}\cdot\tilde{x} + \tilde{l}\cdot x + l\cdot\tilde{x} + \frac{N}{g^2}\iint\left\{\sum_{\alpha=1}^{4}\hat{q}_\alpha(t,t')q_\alpha(t,t') + \frac{1}{2}[q_1(t,t')q_2(t,t')\right.\right.$$

$$\left.\left. + \eta q_3(t,t')q_4(t,t')] - \frac{g^2}{N}\sum_{i=1}^{N}[\hat{q}_1(t,t')\tilde{x}_i(t)\tilde{x}_i(t') + \hat{q}_2(t,t')r_i(t)r_i(t') + \hat{q}_3(t,t')\tilde{x}_i(t)r_i(t') + \hat{q}_4(t,t')r_i(t)\tilde{x}_i(t')]\right\}dt\,dt'\right),$$
(D8)

where we introduced the shorthand notation

$$\mathcal{D}Q \equiv \prod_{\alpha=1}^{4}\frac{1}{2\pi}\frac{N}{g^2}\mathcal{D}q_\alpha\mathcal{D}\hat{q}_\alpha,$$

$$\mathcal{D}X \equiv \mathcal{D}x(t)\mathcal{D}\tilde{x}(t) = \prod_{i=1}^{N}\mathcal{D}x_i(t)\mathcal{D}\tilde{x}_i(t).$$

Equation (D8) can now be expressed as [5,33]

$$Z[l,\tilde{l}] = \int \mathcal{D}Q e^{Nf(q,\hat{q},x,\tilde{x})},$$
(D9)

where

$$f(q,\hat{q},x,\tilde{x}) \equiv G(q,\hat{q}) + \frac{1}{N}\log\int \mathcal{D}X\exp[\mathcal{L}(q,\hat{q},x,\tilde{x})],$$

$$G(q,\hat{q}) \equiv \frac{1}{g^2}\iint\left\{\sum_{\alpha=1}^{4}q_\alpha\hat{q}_\alpha + \frac{1}{2}[q_1q_2 + \eta q_3q_4]\right\}dt\,dt',$$

$$\mathcal{L}(q,\hat{q},x,\tilde{x}) \equiv -S_0[x,\tilde{x}] + \frac{\sigma^2}{2}\tilde{x}\cdot\tilde{x} + \tilde{l}\cdot x + l\cdot\tilde{x} - \sum_{i=1}^{N}\iint[\hat{q}_1(t,t')\tilde{x}_i(t)\tilde{x}_i(t') + \hat{q}_2(t,t')r_i(t)r_i(t')$$

$$+ \hat{q}_3(t,t')\tilde{x}_i(t)r_i(t') + \hat{q}_4(t,t')r_i(t)\tilde{x}_i(t')]dt\,dt'.$$

In the limit of large N we can apply the saddle-point method to Eq. (D9), which amounts to making the approximation

$$Z[l,\tilde{l}] = \int \mathcal{D}Q e^{Nf(q,\hat{q},x,\tilde{x})} \approx e^{Nf(q^0,\hat{q}^0,x,\tilde{x})},$$
(D10)

where q^0 and $\hat{q}^0$ are the values that extremize f. Requiring $\delta f/\delta\hat{q}_\alpha = 0$ leads to

$$q_1^0(t,t') = \frac{g^2}{N}\sum_{i=1}^{N}\langle\tilde{x}_i(t)\tilde{x}_i(t')\rangle_\mathcal{L},$$
(D11)

$$q_2^0(t,t') = \frac{g^2}{N}\sum_{i=1}^{N}\langle r_i(t)r_i(t')\rangle_\mathcal{L},$$
(D12)

$$q_3^0(t,t') = \frac{g^2}{N}\sum_{i=1}^{N}\langle\tilde{x}_i(t)r_i(t')\rangle_\mathcal{L},$$
(D13)

$$q_4^0(t,t') = \frac{g^2}{N}\sum_{i=1}^{N}\langle r_i(t)\tilde{x}_i(t')\rangle_\mathcal{L},$$
(D14)

with the average $\langle\cdot\rangle_\mathcal{L}$ defined as

$$\langle\mathcal{O}\rangle_\mathcal{L} \equiv \frac{\int \mathcal{O}(X)\exp[\mathcal{L}(X)]dX}{\int \exp[\mathcal{L}(X)]dX}.$$

Similarly, from the saddle-point conditions for q_α we obtain

$$\hat{q}_1^0(t,t') = -\frac{1}{2}q_2^0(t,t'), \quad \hat{q}_2^0(t,t') = -\frac{1}{2}q_1^0(t,t'),$$

$$\hat{q}_3^0(t,t') = -\frac{\eta}{2}q_4^0(t,t'), \quad \hat{q}_4^0(t,t') = -\frac{\eta}{2}q_3^0(t,t').$$

Now the right-hand side of Eq. (D10) reads

$$Z[l,\tilde{l}] = \int \mathcal{D}X \exp(-S_0[x,\tilde{x}] - S_{\text{int}}[x,\tilde{x}] + \tilde{l} \cdot x + l \cdot \tilde{x}) \tag{D15}$$

with

$$S_{\text{int}}[x,\tilde{x}] \equiv \frac{1}{2} \iint \left\{ \frac{N}{g^2} \left[q_1^0(t,t')q_2^0(t,t')\eta q_3^0(t,t')q_4^0(t,t') \right] - \sum_{i=1}^{N} \left\{ \left[q_2^0(t,t') + \sigma^2\delta(t-t') \right] \tilde{x}_i(t)\tilde{x}_i(t') \right. \right.$$

$$\left. \left. + q_1^0(t,t')r_i(t)r_i(t')\eta q_4^0(t,t')\tilde{x}_i(t)r_i(t')\eta q_3^0(t,t')r_i(t)\tilde{x}_i(t') \right\} \right\} dt \, dt'. \tag{D16}$$

The auxiliary fields defined in Eqs. (D11)–(D14) are related to physically observable quantities. First, $q_2^0(t,t')$ is related to the population-averaged autocorrelation function

$$C(t,t') \equiv \frac{1}{N} \sum_{i=1}^{N} \langle r_i(t)r_i(t') \rangle$$

by $q_2^0(t,t') = g^2 C(t,t')$. Second, the auxiliary fields $q_3^0(t,t')$ and $q_4^0(t,t')$ are related to the so-called response function, which characterizes the response of the system when it is perturbed by a weak field. More specifically, in our context the response function at site i would be

$$G(t,t') \equiv \left. \frac{\delta\langle r_i(t)\rangle}{\delta h_i(t')} \right|_{h=0}, \tag{D17}$$

where $h_i(t')$ is a time-dependent external field and angular brackets denote the average over the effective action $S[x,\tilde{x}] = S_0[x,\tilde{x}] + S_{\text{int}}[x,\tilde{x}]$ that appears in Eq. (D15). Note that from the definition of response function $G(t,t')$ has to be 0 whenever $t < t'$, due to causality. To see the link between $G(t,t')$ and $q_3(t,t')$ and $q_4(t,t')$, we add an external field $h_i(t)$ for each neuron in Eq. (D1) and evaluate (D17). With the new field the action becomes $S_h[x,\tilde{x}] = S[x,\tilde{x}] - \sum \tilde{x}_i(t)h_i(t)$ and

$$\left. \frac{\delta\langle r_i(t)\rangle}{\delta h_i(t')} \right|_{h=0} = \left. \frac{\delta}{\delta h(t')} \int \mathcal{D}X r_i(t) \exp(-S_h[x,\tilde{x}]) \right|_{h=0}$$

$$= -\left\langle r(t) \left. \frac{\delta S_h}{\delta h_i(t')} \right|_{h=0} \right\rangle = \langle r_i(t)\tilde{x}_i(t') \rangle.$$

Defining the population-averaged response function as

$$G(t,t') \equiv \frac{1}{N} \sum_{i=1}^{N} \langle r_i(t)\tilde{x}_i(t') \rangle,$$

we obtain $q_4^0(t,t') = q_3^0(t',t) = g^2 G(t,t')$.

As for $q_1^0(t,t')$, it can be shown that the presence of vertices like $r_i(t)r_i(t')$ in the action necessarily leads to violation of causality [33]. We thus need to impose $q_1^0(t,t') = 0$ to obtain a physical solution.

We can finally write the interacting action in Eq. (D16) in terms of the physical quantities

$$S_{\text{int}}[x,\tilde{x}] = -\sum_{i=1}^{N} \iint \left\{ \frac{1}{2}\Gamma(t,t')\tilde{x}_i(t)\tilde{x}_i(t') + \eta g^2 G(t,t')\tilde{x}_i(t)r_i(t') \right\} dt \, dt', \tag{D18}$$

where we ignored the term containing $G(t,t')G(t,t')$, which vanishes due to causality, and where we defined

$$\Gamma(t,t') \equiv g^2 C(t,t') + \sigma^2\delta(t-t').$$

Note that the final action involves only interactions that are local in space, which implies that all units are equivalent. This equivalence comes as no surprise because all units are equivalent once we average over all realizations of the connectivity matrix. We can thus drop the irrelevant indices i and focus on the single relevant dynamical variable $x(t)$.

Equation of motion for the average activity

The local action $S[x,\tilde{x}] = S_0[x,\tilde{x}] + S_{\text{int}}[x,\tilde{x}]$, with S_0 and S_{int} given by Eqs. (D6) and (D18), has the form

$$S[x,\tilde{x}] = \iint \left\{ \tilde{x}(t)G_F^{-1}(t-t')x(t') - \eta g^2 \tilde{x}(t)G(t,t')r(t') \right.$$
$$\left. - \tfrac{1}{2}\Gamma(t,t')\tilde{x}(t)\tilde{x}(t') \right\} dt\, dt' \qquad (D19)$$

where for later convenience we have introduced the inverse of the free propagator $G_F^{-1}(t-t')$. The free propagator $G_F(t-t')$ is just the Green's function associated with the operator $d/dt + 1$,

$$\left(\frac{d}{dt}+1\right)G_F(t-t') = \delta(t-t'),$$

and is related to its inverse through $\int G_F^{-1}(t-s)G_F(s-t')ds = \delta(t-t')$, which is automatically satisfied if

$$G_F^{-1}(t-t') = \delta(t-t')\left(\frac{d}{dt'}+1\right).$$

From the original stochastic system (D1) and its associated Martin–Siggia–Rose–Janssen–de Dominicis action (D2), we infer that the equation of motion associated with the action (D19) is

$$\dot{x}(t) = -x(t) + \eta g^2 \int_{-\infty}^{t} G(t,s)r(s)ds + \varphi(t), \qquad (D20)$$

where $\varphi(t)$ is a source of noise with autocorrelation

$$\langle\varphi(t)\varphi(t')\rangle = \Gamma(t,t') = g^2 C(t,t') + \sigma^2 \delta(t-t').$$

This relation has to be consistent with the dynamics generated by Eq. (D20), that is, the noise $\varphi(t)$ has to be such that the firing activity $r(t)$ has autocorrelation $C(t,t')$.

We can go further and write a self-consistent relation involving the two-point functions $C(t,t')$ and $G(t,t')$. A starting point to derive them are the identities

$$\frac{\delta x(t)}{\delta x(t')} = \frac{\delta \tilde{x}(t)}{\delta \tilde{x}(t')} = \delta(t-t'), \quad \frac{\delta \tilde{x}(t)}{\delta x(t')} = \frac{\delta x(t)}{\delta \tilde{x}(t')} = 0,$$

from which we can obtain relations such as

$$\left\langle \frac{\delta x(t)}{\delta x(t')} \right\rangle \equiv \int \mathcal{D}X \frac{\delta x(t)}{\delta x(t')} \exp\{-S[x(t),\tilde{x}(t)]\}$$
$$= \left\langle x(t)\frac{\delta S}{\delta x(t')} \right\rangle = \delta(t-t').$$

Other relations follow analogously:

$$\left\langle x(t)\frac{\delta S}{\delta x(t')} \right\rangle = \delta(t-t'), \qquad (D21a)$$

$$\left\langle x(t)\frac{\delta S}{\delta \tilde{x}(t')} \right\rangle = 0, \qquad (D21b)$$

$$\left\langle \tilde{x}(t)\frac{\delta S}{\delta \tilde{x}(t')} \right\rangle = \delta(t-t'), \qquad (D22a)$$

$$\left\langle \tilde{x}(t)\frac{\delta S}{\delta x(t')} \right\rangle = 0, \qquad (D22b)$$

We now apply the identities (D21) and (D22) for the action (D19). In particular, we use the identities involving

$$\frac{\delta S}{\delta \tilde{x}(t')} = \dot{x}(t) + x(t) - \eta g^2 \int_{-\infty}^{t} G(t,s)r(s)ds$$
$$- \int \Gamma(t,s)\tilde{x}(s)ds$$

and we define the autocorrelation and response function of the activation field $x(t)$

$$\Delta(t,t') \equiv \langle x(t)x(t')\rangle, \quad R(t,t') \equiv \langle x(t)\tilde{x}(t')\rangle.$$

Equations (D21b) and (D22a) then become, respectively,

$$\frac{\partial}{\partial t}\Delta(t,t') = -\Delta(t,t') + \sigma^2 R(t',t)\eta g^2 \int_0^t G(t,s)\langle r(s)x(t')\rangle ds + g^2 \int_0^{t'} R(t',s)C(t,s)ds, \qquad (D23)$$

$$\frac{\partial}{\partial t}R(t,t') = -R(t,t') + \delta(t-t') + \eta g^2 \int_{t'}^{t} G(t,s)G(s,t')ds, \qquad (D24)$$

where in Eq. (D24) we have used $\langle \tilde{x}(t)\tilde{x}(t')\rangle = 0$. It can be shown that the remaining identities in Eqs. (D21) and (D22), which involve $\delta S/\delta x$, do not provide additional information [73]. Note that $\Delta(t,t')$ has a cusp at $t = t'$ due to the term $\sigma^2 R(t',t)$, which from (D22) we know it must be of the form $R(t,t') \propto \Theta(t-t')$, with $\Theta(t)$ being the step function. More specifically,

$$\left[\frac{\partial}{\partial t}\Delta(t,t')\right]_{t'=t^+}^{t'=t^-} = \sigma^2 [R(t',t)]_{t'=t^+}^{t'=t^-} = -\sigma^2.$$

Moreover, the symmetry of $\Delta(t,t')$ around $t = t'$ implies $\lim_{t'\to t^-}\partial_t\Delta(t,t') = -\lim_{t'\to t^+}\partial_t\Delta(t,t')$, which leads to the relation $\lim_{t'\to t^-}\partial_t\Delta(t,t') = -\sigma^2/2$. The amplitude of external noise thus determines the slope of the autocorrelation of $x(t)$ at zero-time lag. This is the only dependence on σ^2 of the solutions of (D23) and (D24).

Equations (D23) and (D24) cannot be solved in a closed form except for $\eta = 0$ [1], but perturbative solutions can be found by expanding the nonlinearity $r(t) = \phi(x)$ in power series of $x(t)$ and then solving the resulting hierarchy of equations, which involve correlations and response functions of increasingly larger order. The problem becomes unwieldy except for the linear case where $r(t) = x(t)$. In that case, $C(t,t') = \Delta(t,t')$, $G(t,t') = R(t,t')$, and Eqs. (D23) and (D24) form a closed system of

integro-differential equations

$$\frac{\partial}{\partial t}\Delta(t,t') = -\Delta(t,t') + \sigma^2 R(t',t) + \eta J^2 \int_0^t R(t,s)\Delta(s,t')ds + g^2 \int_0^{t'} R(t',s)\Delta(t,s)ds, \tag{D25}$$

$$\frac{\partial}{\partial t}R(t,t') = -R(t,t') + \delta(t-t') + \eta g^2 \int_{t'}^t R(t,s)R(s,t')ds. \tag{D26}$$

[1] H. Sompolinsky, A. Crisanti, and H. J. Sommers, Phys. Rev. Lett. **61**, 259 (1988).

[2] C. van Vreeswijk and H. Sompolinsky, Neural Comput. **10**, 1321 (1998).

[3] N. Brunel, J. Comput. Neurosci. **8**, 183 (2000).

[4] D. V. Buonomano and W. Maass, Nat. Rev. Neurosci. **10**, 113 (2009).

[5] T. Toyoizumi and L. F. Abbott, Phys. Rev. E **84**, 051908 (2011).

[6] D. Sussillo and L. F. Abbott, Neuron **63**, 544 (2009).

[7] M. N. Shadlen and W. T. Newsome, J. Neurosci. **18**, 3870 (1998).

[8] D. J. Amit and N. Brunel, Cereb. Cortex **7**, 237 (1997).

[9] H. Markram, J. Lübke, M. Frotscher, and B. Sakmann, J. Physiol. **500**, 409 (1997).

[10] S. Song, P. J. Sjöström, M. Reigl, S. Nelson, and D. B. Chklovskii, PLoS Biol. **3**, e68 (2005).

[11] R. Perin, T. K. Berger, and H. Markram, P. Natl. Acad. Sci. USA **108**, 5419 (2011).

[12] H. Ko, S. B. Hofer, B. Pichler, K. A. Buchanan, P. J. Sjöström, and T. D. Mrsic-Flogel, Nature (London) **473**, 87 (2011).

[13] K. D. Harris and T. D. Mrsic-Flogel, Nature (London) **503**, 51 (2013).

[14] Y. Wang, H. Markram, P. H. Goodman, T. K. Berger, J. Ma, and P. S. Goldman-Rakic, Nat. Neurosci. **9**, 534 (2006).

[15] A. Crisanti and H. Sompolinsky, Phys. Rev. A **36**, 4922 (1987).

[16] J. T. Chalker and B. Mehlig, Phys. Rev. Lett. **81**, 3367 (1998).

[17] B. Mehlig and J. T. Chalker, J. Math Phys. **41**, 3233 (2000).

[18] C. Huang and B. Doiron, Curr. Opin. Neurobiol. **46**, 31 (2017).

[19] K. Rajan, L. F. Abbott, and H. Sompolinsky, Phys. Rev. E **82**, 011903 (2010).

[20] J. Kadmon and H. Sompolinsky, Phys. Rev. X **5**, 041030 (2015).

[21] O. Harish and D. Hansel, PLoS Comput. Biol. **11**, e1004266 (2015).

[22] F. Mastrogiuseppe and S. Ostojic, PLoS Comput. Biol. **13**, e1005498 (2017).

[23] G. Wainrib and J. Touboul, Phys. Rev. Lett. **110**, 118101 (2013).

[24] J. Ginibre, J. Math Phys. **6**, 440 (1965).

[25] V. L. Girko, Teor. Ver. Prim. **29**, 669 (1984).

[26] T. Tao, V. Vu, and M. Krishnapur, Ann. Probab. **38**, 2023 (2010).

[27] V. L. Girko, Teor. Ver. Prim. **30**, 640 (1985).

[28] H. J. Sommers, A. Crisanti, H. Sompolinsky, and Y. Stein, Phys. Rev. Lett. **60**, 1895 (1988).

[29] A. A. Naumov, Vestnik Moskov. Univ. Ser. XV Vychisl. Mat. Kibernet. **1**, 31 (2013).

[30] H. H. Nguyen and S. O'Rourke, Int. Math. Res. Not. **2015**, 7620 (2015).

[31] J. Schuecker, S. Goedeke, and M. Helias, arXiv:1603.01880.

[32] L. N. Trefethen and M. Embree, *Spectra and Pseudospectra: The Behavior of Nonnormal Matrices and Operators* (Princeton University Press, Princeton, 2005).

[33] H. Sompolinsky and A. Zippelius, Phys. Rev. B **25**, 6860 (1982).

[34] B. Bravi, P. Sollich, and M. Opper, J. Phys. A: Math. Theor. **49**, 194003 (2016).

[35] G. Hennequin, T. P. Vogels, and W. Gerstner, Phys. Rev. E **86**, 011909 (2012).

[36] J.-P. Bouchaud, L. F. Cugliandolo, J. Kurchan, and M. Mézard, in *Spin Glasses and Random Fields*, edited by A. P. Young (World Scientific, Singapore, 1998), Chap. 6, pp. 161–223.

[37] J. J. Hopfield, Proc. Natl. Acad. Sci. USA **79**, 2554 (1982).

[38] D. J. Amit, H. Gutfreund, and H. Sompolinsky, Phys. Rev. A **32**, 1007 (1985).

[39] J. A. Hertz, G. Grinstein, and S. A. Solla, in *Neural Networks for Computing*, edited by J. S. Denker, AIP Conf. Proc. No. 151 (American Institute of Physics, Woodbury, 1986), pp. 212–218.

[40] B. Derrida, E. Gardner, and A. Zippelius, Europhys. Lett. **4**, 167 (1987).

[41] C. van Vreeswijk and H. Sompolinsky, Science **274**, 1724 (1996).

[42] A. Litwin-Kumar and B. Doiron, Nat. Neurosci. **15**, 1498 (2012).

[43] M. Stern, H. Sompolinsky, and L. F. Abbott, Phys. Rev. E **90**, 062710 (2014).

[44] A. Roxin, Front. Comput. Neurosci. **5**, 8 (2011).

[45] L. Zhao, B. Beverlin, T. Netoff, and D. Nykamp, Front. Comput. Neurosci. **5**, 28 (2011).

[46] C. Bimbard, E. Ledoux, and S. Ostojic, Phys. Rev. E **94**, 062207 (2016).

[47] N. Brunel, Nat. Neurosci. **19**, 749 (2016).

[48] S. Ganguli, D. Huh, and H. Sompolinsky, Proc. Natl. Acad. Sci. USA **105**, 18970 (2008).

[49] B. K. Murphy and K. D. Miller, Neuron **61**, 635 (2009).

[50] M. S. Goldman, Neuron **61**, 621 (2008).

[51] G. Hennequin, T. P. Vogels, and W. Gerstner, Neuron **82**, 1394 (2014).

[52] Y. Ahmadian, F. Fumarola, and K. D. Miller, Phys. Rev. E **91**, 012820 (2015).

[53] M. Mézard, G. Parisi, and M. Virasoro, *Spin Glass Theory and Beyond: An Introduction to the Replica Method and Its Applications* (World Scientific, Singapore, 1987), Vol. 9.

[54] L. F. Cugliandolo and J. Kurchan, Phys. Rev. Lett. **71**, 173 (1993).

[55] L. F. Cugliandolo and D. S. Dean, J. Phys. A: Math. Gen. **28**, 4213 (1995).

[56] G. Iori and E. Marinari, J. Phys. A: Math. Gen. **30**, 4489 (1997).

[57] E. Marinari and D. A. Stariolo, J. Phys. A: Math. Gen. **31**, 5021 (1998).

[58] S. Lefort, C. Tomm, J. C. F. Sarria, and C. C. Petersen, Neuron **61**, 301 (2009).

[59] J. D. Murray, A. Bernacchia, D. J. Freedman, R. Romo, J. D. Wallis, X. Cai, C. Padoa-Schioppa, T. Pasternak, H. Seo, D. Lee, and X. J. Wang, Nat. Neurosci. **17**, 1661 (2014).

[60] H. Wang, G. G. Stradtman, X. J. Wang, and W. J. Gao, Proc. Natl. Acad. Sci. USA **105**, 16791 (2008).

[61] G. N. Elston, Cereb. Cortex **13**, 1124 (2003).

[62] K. Rajan and L. F. Abbott, Phys. Rev. Lett. **97**, 188104 (2006).

[63] S. Ostojic, Nat. Neurosci. **17**, 594 (2014).

[64] J. Aljadeff, M. Stern, and T. Sharpee, Phys. Rev. Lett. **114**, 088101 (2015).

[65] A. Kuczala and T. O. Sharpee, Phys. Rev. E **94**, 050101 (2016).

[66] J. Aljadeff, D. Renfrew, and M. Stern, J. Math. Phys. **56**, 103502 (2015).

[67] A. P. Prudnikov, Y. A. Brychkov, and O. I. Marichev, *Integrals and Series* (Gordon and Breach, New York, 1992), Vol. 2.

[68] C. M. Bender and S. A. Orszag, *Advanced Mathematical Methods for Scientists and Engineers* (Springer, Berlin, 1999).

[69] I. S. Gradshteyn and I. M. Ryzhik, in *Table of Integrals, Series, and Products*, 7th ed., edited by A. Jeffrey and D. Zwillinger (Elsevier, Amsterdam, 2007), p. 496.

[70] P. C. Martin, E. Siggia, and H. Rose, Phys. Rev. A **8**, 423 (1973).

[71] H.-K. Janssen, Z. Phys. B **23**, 377 (1976).

[72] C. Chow and M. Buice, J. Math. Neurosci. **5**, 8 (2015).

[73] L. F. Cugliandolo, Out of equilibrium dynamics of complex systems, lecture notes, King's College, 2013 (unpublished).

[74] C. De Dominicis, Phys. Rev. B **18**, 4913 (1978).